

Modified Inception V3 based blockage fault diagnosis of centrifugal pump

MS (Research) Thesis

By

DEEPAK KUMAR



**DEPARTMENT OF MECHANICAL ENGINEERING
INDIAN INSTITUTE OF TECHNOLOGY INDORE**

JUNE, 2024

Modified InceptionV3 based blockage fault diagnosis of centrifugal pump

A THESIS

*Submitted in fulfilment of the
requirements for the award of the degree
of*

Master of Science (Research)

by

DEEPAK KUMAR



**DEPARTMENT OF MECHANICAL ENGINEERING
INDIAN INSTITUTE OF TECHNOLOGY INDORE**

JUNE, 2024




INDIAN INSTITUTE OF TECHNOLOGY INDORE

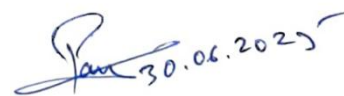
CANDIDATE'S DECLARATION

I hereby certify that the work which is being presented in the thesis entitled **Modified InceptionV3 based blockage fault diagnosis of centrifugal pump** in the fulfilment of the requirements for the award of the degree of **MASTER OF SCIENCE (RESEARCH)** and submitted in the **DEPARTMENT OF MECHANICAL ENGINEERING, Indian Institute of Technology Indore**, is an authentic record of my own work carried out during the time period from August 2022 to June 2024 under the supervision of **Dr. Pavan Kumar Kankar**, Professor in Department of Mechanical Engineering, Indian Institute of Technology , Indore.

The matter presented in this thesis has not been submitted by me for the award of any other degree of this or any other institute.


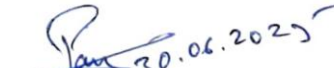



DEEPAK KUMAR
(Student)

This is to certify that the above statement made by the candidate is correct to the best of my/our knowledge.


30.06.2025

Dr. Pavan Kumar Kankar
(Thesis Supervisor)

Deepak Kumar has successfully given his MS (Research) Oral Examination held on **30.06.2025**.

 11.07.2025 Signature of Chairperson (OEB) with date	 30.06.2025 Signature(s) of Thesis Supervisor(s) with date
 11.07.2025 Signature of Convener, DPGC with date	 Signature of Head of Discipline with date Prof. Dharmakaran Shanmugam HoD, MechE 11-July-2025

ACKNOWLEDGEMENTS

First and foremost, I would like to express my deepest gratitude to my professor and guide, **Dr. Pavan Kumar Kankar**, whose unwavering support, invaluable guidance, and insightful feedback have been instrumental throughout my research journey. His encouragement and expertise have been the cornerstone of this thesis.

I am immensely thankful to my lab mates, **Nagendra Singh Ranawat, Vinod Singh, and Apoorva Tripathi**, for their camaraderie, collaborative spirit, and the stimulating discussions that have enriched my research experience. Their assistance and constructive critiques have been invaluable.

A special thanks to **Suresh Bhagore**, our lab assistant, for his invaluable help with paperwork and workshop tasks. His support has been crucial in the smooth execution of my research.

I am deeply grateful to my parents and sisters for their unconditional love, unwavering support, and constant encouragement throughout my academic journey. Their sacrifices and belief in me have been my greatest source of strength.

Special thanks to my love who lives in my heart. Your presence and support, even from afar, have been a constant source of motivation and inspiration.

I extend my heartfelt thanks to my friends Manik, Ispارش, Zen, Harsh, Ridham, Shubham Jain, Shubham Garg, Prosenjit, Arbaaz, Rahul, and Mahesh for their moral support and for always being there during the highs and lows of this journey. Your encouragement and belief in me have meant the world.

I would also like to extend my gratitude to IIT Indore and the Ministry of Human Resource Development (MHRD) for providing excellent facilities and a conducive environment for research. The resources and infrastructure at the System Dynamics Lab have significantly contributed to the successful completion of my work.

Finally, I would like to acknowledge everyone who directly or indirectly supported me throughout this endeavour. Your contributions have been deeply appreciated.

Thank you, everyone...!!

Deepak Kumar

Dedicated to my father for believing in me

Abstract

Centrifugal pumps play a vital role across numerous industries—including water treatment, manufacturing, oil and gas, and chemical processing—but remain vulnerable to hydraulic faults that can severely degrade performance and precipitate unplanned shutdowns. Among these, blockage faults in the suction line, discharge line, or both are often overlooked in diagnostics despite their potential to trigger catastrophic pump failures. Prompt and accurate detection of blockage severity is therefore essential for maintaining pump reliability, ensuring operational safety, and minimizing maintenance costs. In this work, we present a deep learning-based framework that relies solely on suction pressure signals for the classification and severity assessment of blockage conditions. Suction pressure time-series are first transformed into two-dimensional time–frequency scalograms via the Continuous Wavelet Transform (CWT), which captures the transient and nonstationary features of the signal with higher resolution than traditional FFT or STFT approaches. These scalogram images serve as inputs to a modified InceptionV3 Convolutional Neural Network (CNN), chosen for its proven efficacy in image-based recognition tasks. To better capture subtle nonlinear patterns indicative of different blockage scenarios, we enhance the standard InceptionV3 architecture by introducing Exponential Linear Unit (ELU) activations alongside conventional ReLUs. ELUs mitigate the vanishing gradient problem and promote faster convergence by producing activations centered closer to zero. Our modifications also include parallel ReLU/ELU branches, strategic dropout layers to guard against overfitting, and an optimized training regimen featuring data augmentation, adaptive learning-rate scheduling, and early stopping. Experimental data were collected from a centrifugal pump test rig at IIT Indore, encompassing 35 distinct operating conditions: a healthy baseline, six levels of suction-only blockages, four discharge-only blockages, and 24 combined suction–discharge blockages. Training this enriched CNN on the CWT scalograms yielded a training accuracy of 99.68%, validation accuracy of 95.48%, and test accuracy of 95.36%, representing a substantial improvement over the 81.82% test accuracy achieved by the unmodified InceptionV3 baseline at 2000 RPM. The proposed methodology demonstrates the modified InceptionV3 model’s efficacy in classifying various blockage conditions, making it a potent tool for predictive maintenance in industrial settings.

List of publication

Deepak Kumar, Nagendra Singh Ranawat, Pavan Kumar Kankar, Ankur Miglani, “InceptionV3 based blockage fault diagnosis of centrifugal pump”, Advanced Engineering Informatics, Volume 65, Part A, 2025, 103181 ISSN 1474-0346, <https://doi.org/10.1016/j.aei.2025.103181>.
(<https://www.sciencedirect.com/science/article/pii/S1474034625000746>)

TABLE OF CONTENTS

LIST OF TABLES	17
LIST OF FIGURES	18
ACRONYMS	20
<hr/>	
CHAPTER – 1: INTRODUCTION.....	21
<i>1.1 Background: Description of centrifugal pump</i>	21
<i>1.2 Application</i>	22
<i>1.3 Working of centrifugal pump</i>	24
<i>1.4 Types of faults and causes in centrifugal pump</i>	26
<i>1.5 Thesis outline</i>	27
<hr/>	
CHAPTER – 2: Literature survey.....	29
<i>2.1 Previous Literature</i>	29
<i>2.2 Salient Observations and Research Gaps</i>	30
<i>2.3 Research objective</i>	31
<hr/>	
CHAPTER – 3: Experimental Setup.....	33
<i>3.1 Test procedure</i>	35
<i>3.2 Performance of pump</i>	36
<hr/>	
CHAPTER – 4: Blockage faults classification.....	39
<i>4.1 Classification methodology</i>	39
<i>4.2 Continuous Wavelet Transform</i>	40
<hr/>	
CHAPTER – 5: Deep CNN Model architecture.....	45
<i>5.1 Training Methodology</i>	48
<i>5.2 Hyperparameter selection</i>	49
<i>5.3 Dataset similarity analysis</i>	52

5.4 Model performance evaluation	53
<hr/>	
CHAPTER – 6: Results and discussion	55
6.1 Classification of blockage faults using InceptionV3 Model....	55
6.2 Classification of blockage faults using Modified InceptionV3 Model	60
6.3 Comparison.....	63
<hr/>	
CHAPTER – 7: Conclusion and future work.....	71
7.1 Conclusion	71
7.2 Limitation.....	71
7.3 Future Work	72
<hr/>	
APPENDIX – A: Deep CNN Basic Structure.....	75
References.....	83

LIST OF TABLES

Table 1: Different types of faults and their causes associated with centrifugal pump	27
Table 2: Details of blockage faults induced in centrifugal pump	36
Table 3: Selection of split ratio (Training: Validation: Test) for modified inceptionV3 model based on hyperparameter tuning.	50
Table 4: Hyperparameter tuning in Modified InceptionV3 model.	51
Table 5: Performance comparison of modified inceptionV3 with other pre-trained models at 2000RPM, 1750RPM and 1500RPM.....	65
Table 6: Performance comparison of modified inceptionV3 with the combination of ReLU with other Activation Functions at 2000RPM.....	66
Table 7: Results of hyper-parameter optimization for five-fold cross validation.....	66
Table 8: Results of five-fold cross-validation.....	67
Table 9: Comparative study of current work with other literature...	68

LIST OF FIGURES

Figure 1: Sketch diagram of centrifugal pump	21
Figure 2: Diagrammatic Representation of working of centrifugal pump	24
Figure 3: CAD model of the experimental facility to simulate blockage fault in a centrifugal pump, developed in the System Dynamics Lab of IIT Indore (India).....	34
Figure 4: CAD model of (a) Notch plate with 10 notches of suction side butterfly valve, (b) Notch plate with 7 notches of discharge side butterfly valve, (c) Wafer-style body type butterfly valve.	34
Figure 5: Pump performance parameter (a) Suction Pressure, (b) Discharge Pressure, (c) Flowrate, (d) Head, (e) Head vs Flowrate (H-Q) curve. (For each plot, mean values of parameters are taken). Notation: SDB1510 means the SDB15 curve at SB10 in the plots.....	38
Figure 6: Methodology adopted for blockage fault classification in a centrifugal pump.	39
Figure 7: CWT of suction pressure signals (a) Healthy condition and severity level of suction blockage namely (b) SB10, (c) SB30, and (d) SB60.....	41
Figure 8: CWT of suction pressure signals at different severity levels of discharge blockages, namely (a) DB15, (b) DB30, (c) DB45, and (d) DB60.	42
Figure 9: CWT of suction pressure signals at different severity levels of discharge blockages, namely (a) SDB1510, (b) SDB1530, and (c) SDB1560.	42
Figure 10: CWT of suction pressure signals at different severity levels of discharge blockages, namely (a) SDB3010, (b) SDB3030, and (c) SDB3060.	43
Figure 11: CWT of suction pressure signals at different severity levels of discharge blockages, namely (a) SDB4510, (b) SDB4530, and (c) SDB4560.	43
Figure 12: CWT of suction pressure signals at different severity levels of discharge blockages, namely (a) SDB6010, (b) SDB6030, and (c) SDB6060.	43
Figure 13: Basic module of (a) InceptionV3, (b) Modified InceptionV3.....	45
Figure 14: Modified InceptionV3 network with no. of kernel and size of kernel. Here, only ReLU layer Module can be consider as InceptionV3 network.	47

Figure 15: Complete layout of Modified InceptionV3 model-based classifier.	48
Figure 16: Euclidean Distance measures the dissimilarity between the training and test images. Higher values indicate greater dissimilarity.....	52
Figure 17: Universal Quality Index (UQI) measures the similarity between the training and test images. Values close to 1 indicate high similarity, while values near 0 indicate low similarity.	52
Figure 18: Training and Validation curve for InceptionV3 model showing (a) Accuracy, (b) Loss.....	55
Figure 19: Overall performance parameter of inceptionV3 (values are in percentage).....	57
Figure 20: Confusion matrix for test data classified by InceptionV3 model.	59
Figure 21: Training and Validation curve for Modified InceptionV3 model showing (a) Accuracy, (b) Loss.	60
Figure 22: Overall performance parameter of inceptionV3 (values are in percentage).....	61
Figure 23: Confusion matrix for test data classified by Modified InceptionV3 model.	62
Figure 24: Comparison of performance of IncetionV3 and Modified InceptionV3 model based on (a) Performance parameter and (b) Size and time.	64
Figure 25: Comparison of F1 - Score of IncetionV3 and Modified InceptionV3 model in case of (a) DB, (b) SB, (c) SDB1510 to SDB3060, (d) SDB4510 to SDB6060.	65

ACRONYMS

ML	Machine Learning
SVM	Support Vector Machine
ANN	Artificial Neural Network
CNN	Convolutional Neural Network
DNN	Deep Neural Network
FFT	Fast Fourier Transform
STFT	Short Time Frequency Transform
CWT	Continuous Wavelet Transform
ReLU	Rectified Linear Unit
ELU	Exponential Linear Unit

CHAPTER – 1: INTRODUCTION

1.1 Background: Description of centrifugal pump

A centrifugal pump is a hydraulic machine that converts mechanical energy into hydraulic energy through the action of centrifugal force on a fluid. The primary function of a centrifugal pump is to impart velocity to a liquid using rotational motion, which is then converted into flow. These pumps are composed of various mechanical components that ensure their proper operation as shown in Figure1[1].

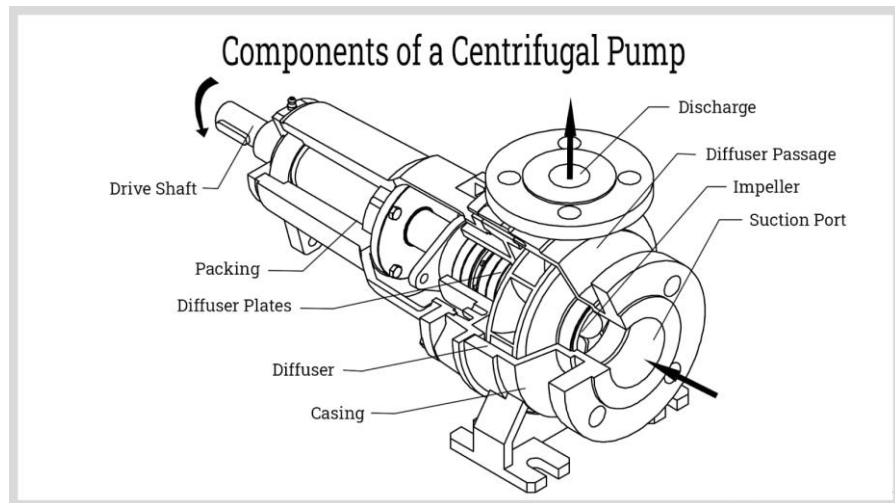


Figure 1: Sketch diagram of centrifugal pump

The central part of the pump is the shaft, which rotates with the impeller and is connected to the prime mover for power. The impeller, with its backward-curved vanes, imparts velocity to the liquid and is enclosed in an airtight casing. The casing, surrounding the impeller, converts the kinetic energy of the water into pressure energy before it exits through the delivery pipe. There are different types of casings, such as volute, vortex, and casings with guide blades, each designed to optimize the pressure and flow characteristics of the pump.

The suction pipe, equipped with a strainer and a foot valve, prevents foreign objects from entering and ensures a unidirectional flow. The delivery valve directs the water to the desired height. Material selection for manufacturing centrifugal pumps is crucial, considering factors like strength, wear resistance, corrosion resistance, and cost. Common materials include cast iron, stainless steel, bronze, and various composites, each chosen based on the specific requirements of the pump's application.

Centrifugal pumps come in various types, including 12V pumps, chemical pumps, radial pumps, axial pumps, mixed flow pumps, single suction pumps, double suction pumps, single volute pumps, trash pumps, vertical pumps, and well pumps. Each type serves specific

applications, ranging from domestic water supply and industrial processes to handling abrasive and corrosive materials. The choice of pump type depends on factors such as flow rate, pressure requirements, and the nature of the fluid being pumped.

1.2 Application

Centrifugal pumps are widely used across various industries and applications due to their efficiency, versatility, and reliability. Following are some applications:

- **Water Supply Systems**
 - **Municipal Water Supply:** Centrifugal pumps are essential in municipal water supply systems for pumping water from treatment plants to storage facilities and then to the distribution networks serving residential, commercial, and industrial areas.
 - **Booster Systems:** These pumps help maintain consistent water pressure in high-rise buildings and large facilities by boosting the water pressure as needed.
 - **Domestic Water Supply:** Centrifugal pumps are used in household water systems to ensure an adequate supply of water from wells, reservoirs, or other sources.
- **Industrial Applications**
 - **Manufacturing Plants:** Used for cooling systems, boiler feedwater, and transferring various fluids in manufacturing processes.
 - **Chemical Industry:** Handles the transfer of chemicals, solvents, and other corrosive materials. Specialized chemical pumps are designed to resist corrosion and chemical reactions.
 - **Oil and Gas Industry:** Used in oil refineries for pumping crude oil, fuel, lubricants, and other petroleum products. They also play a role in transporting oil through pipelines and in offshore platforms.
- **Food and Beverage Industry**
 - **Food Processing:** Pumps are used for transferring liquids, semi-liquids, and slurry mixtures in food production. They handle beverages like milk, juice, and syrups.
 - **Breweries:** Used in the brewing process to transfer wort, beer, and cleaning solutions.
 - **Dairy Industry:** Essential for transferring milk, cream, and other dairy products from one process stage to another.
- **Agriculture and Irrigation**
 - **Irrigation Systems:** Centrifugal pumps are used to draw water from rivers, lakes, or wells to irrigate crops. They ensure an efficient and steady supply of water to fields.

- Fertilizer Distribution: These pumps can handle slurry mixtures and liquid fertilizers, ensuring even distribution across agricultural fields.
- Fire Protection Systems
 - Firefighting: Installed in buildings, factories, and industrial complexes, these pumps provide a reliable water supply for sprinkler systems and fire hydrants.
 - Emergency Systems: Portable centrifugal pumps are used by fire departments for emergency water supply in firefighting operations.
- HVAC Systems (Heating, Ventilation, and Air Conditioning)
 - Cooling Towers: Used to circulate water in cooling towers and chiller systems in commercial and industrial buildings.
 - Boiler Feedwater: Ensures a steady supply of water to boilers, which is crucial for heating systems in large buildings and industrial processes.
 - Circulating Systems: Maintain the flow of heated or cooled water throughout HVAC systems.
- Wastewater Management
 - Sewage Treatment: Centrifugal pumps handle the transfer and treatment of sewage and wastewater. They are used in various stages of the treatment process, from raw sewage pumping to sludge handling.
 - Effluent Treatment: Pumps play a crucial role in treating industrial effluents before they are discharged into water bodies or reused.
- Mining and Construction
 - Dewatering: Essential for removing water from construction sites, mines, and tunnels to maintain dry working conditions.
 - Slurry Transport: Used to transport slurry mixtures of water and solid particles, such as those found in mining operations and construction sites.
- Marine Applications
 - Ballast Systems: Centrifugal pumps manage ballast water in ships, ensuring stability and proper buoyancy.
 - Cooling Systems: Used in marine engines to circulate cooling water.
 - Bilge Pumps: Remove water that accumulates in the bilge of a ship, ensuring the vessel remains stable and dry.

- **Pharmaceutical and Cosmetics Industry**
 - **Drug Production:** Involved in the transfer of liquid pharmaceuticals and intermediates during the manufacturing process.
 - **Cosmetic Production:** Used for mixing and transferring lotions, creams, and other cosmetic products.
- **Energy and Power Generation**
 - **Hydroelectric Plants:** Used in auxiliary systems for maintaining cooling and lubrication circuits.
 - **Thermal Power Plants:** Circulate cooling water and feed water for boilers, ensuring efficient operation of the plant.
- **Cryogenic Applications**
 - **LNG Plants:** Centrifugal pumps are designed to handle extremely low temperatures, making them suitable for pumping liquid natural gas (LNG) and other cryogenic fluids.
 - **Medical and Research Labs:** Used in systems that require the transfer of liquid nitrogen and other cryogenic substances.

1.3 Working of centrifugal pump

Centrifugal pumps operate based on the principle of converting rotational kinetic energy, typically from a motor, into hydrodynamic energy in the form of fluid flow. The detailed explanation of the working mechanism of a centrifugal pump shown in Figure 2:

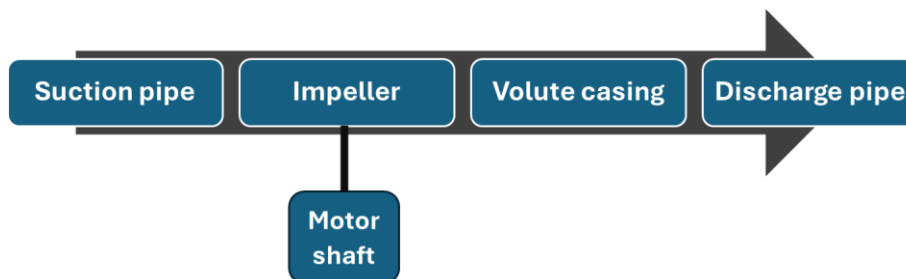


Figure 2: Diagrammatic Representation of working of centrifugal pump

- **Processes:**
 - i. **Suction Pipe:** Fluid enters the pump.
 - ii. **Impeller:** Rotates and imparts kinetic energy to the fluid.
 - iii. **Volute Casing/Diffuser:** Converts kinetic energy to pressure energy.
 - iv. **Discharge Pipe:** Fluid exits the pump.

➤ Suction Process

When the pump starts, the impeller rotates, creating a low-pressure region at the eye (centre) of the impeller. This low-pressure region causes the fluid to flow from the suction pipe into the impeller due to the pressure difference between the fluid source and the impeller eye.

➤ Impeller Action

As the fluid enters the impeller, it encounters the impeller blades. The rotational motion of the impeller imparts kinetic energy to the fluid, causing it to move outward along the impeller blades. This movement is due to the centrifugal force created by the impeller's rotation.

➤ Conversion of Kinetic Energy to Pressure Energy

As the fluid moves outward from the center of the impeller, its velocity increases, and kinetic energy is imparted to the fluid. When the fluid reaches the outer edge of the impeller, it enters the pump casing. The design of the pump casing (typically volute or diffuser) plays a crucial role in converting the kinetic energy of the fluid into pressure energy.

- Volute Casing: A spiral-shaped casing that gradually increases in area as it approaches the discharge port. This design helps in converting the high-velocity fluid from the impeller into high-pressure fluid by gradually reducing the fluid's velocity.
- Diffuser: Consists of a series of stationary vanes surrounding the impeller. The vanes guide the fluid flow and convert kinetic energy into pressure energy by slowing down the fluid in a controlled manner.

➤ Discharge Process

After the fluid's kinetic energy is converted into pressure energy, the high-pressure fluid is directed towards the discharge pipe. The fluid then flows out of the pump and into the discharge system.

➤ Continuous Operation

The pump operates continuously as long as the impeller keeps rotating. The process of fluid entering the pump through the suction pipe, gaining energy from the impeller, and exiting through the discharge pipe happens in a continuous cycle, ensuring a steady flow of fluid.

➤ Factors Affecting Performance

Several factors influence the performance of a centrifugal pump:

- Impeller Design: The shape, size, and number of impeller blades affect the pump's efficiency and the amount of energy imparted to the fluid.

- **Pump Speed:** The rotational speed of the impeller determines the amount of kinetic energy transferred to the fluid. Higher speeds generally increase the flow rate and pressure.
- **Fluid Properties:** The viscosity, density, and temperature of the fluid can impact the pump's performance. Centrifugal pumps are typically designed to handle fluids with specific properties.
- **System Design:** The design of the suction and discharge systems, including the length and diameter of the pipes, presence of valves, and overall system pressure, can affect the pump's efficiency and performance.

➤ Priming of Centrifugal Pump

Before starting, a centrifugal pump often requires priming, which is the process of removing air from the pump and suction line. Priming ensures that the pump casing and suction line are filled with fluid, preventing air pockets that can impede pump operation and cause cavitation.

The benefits of centrifugal pumps include reduced friction, corrosion resistance, energy efficiency, smooth flow, reliability, low maintenance, size versatility, application versatility, and elimination of leakage risk. However, they also have drawbacks such as cavitation, blockage, impeller wear, potential corrosion, surge issues, overheating at low flow, and power consumption.

1.4 Types of faults and causes in centrifugal pump

Centrifugal pumps are widely used in various applications, and like any mechanical equipment, they are prone to faults that can affect their performance and lifespan. Understanding these faults and their causes is crucial for maintaining the reliability and efficiency of the pump.

So, maintaining centrifugal pumps involves regular inspection, lubrication, and checking mechanical and electrical components. Proper maintenance ensures longevity and efficient operation. Overall, centrifugal pumps are essential in many applications, providing reliable and efficient fluid transfer when appropriately chosen and maintained using data driven methods.

Table 1: Different types of faults and their causes associated with centrifugal pump

S.N.	Faults	Description	Causes
1.	Cavitation	Vapor bubbles form and collapse violently.	<ul style="list-style-type: none">• Low suction pressure High fluid temperature.• Excessive pump speed.• Improper pump selection (wrong NPSH).
2.	Bearing Failure	Bearings fail, leading to misalignment and increased friction.	<ul style="list-style-type: none">• Poor lubrication or contaminated lubricant.• Misalignment of pump and motor shaft.• Excessive radial or axial loads.• Wear and tear due to prolonged use.
3.	Seal Leakage	Mechanical seals or packing fail, causing fluid leakage.	<ul style="list-style-type: none">• Worn-out seals or packing.• Improper installation or selection of seals.• Excessive vibration or shaft misalignment.• Abrasive particles in the fluid.
4.	Impeller Wear /Damage	Impeller damage affects pump performance.	<ul style="list-style-type: none">• Handling abrasive or corrosive fluids• Cavitation.• Improperly sized impeller.• Foreign objects entering the pump.
5.	Suction /Discharge Issues	Problems in suction and discharge lines affect flow and pressure.	<ul style="list-style-type: none">• Blockages or obstructions.• Air entrainment or leaks.• Incorrect pipe sizing or length.
6.	Vibration and Noise	Excessive vibration and noise indicate mechanical or hydraulic issues.	<ul style="list-style-type: none">• Misalignment of pump and motor.• Imbalance of impeller.• Loose or worn-out components.• Cavitation or flow turbulence.
7.	Over-heating	Overheating of pump or motor reduces efficiency and can cause failure.	<ul style="list-style-type: none">• Insufficient cooling or ventilation.• Excessive load or high speed.• Bearing failure.• Electrical issues in motor.
8.	Loss of Prime	Pump loses its prime and cannot draw fluid into the impeller.	<ul style="list-style-type: none">• Air leaks in suction line.• Insufficient fluid level.• Obstructions in suction line.• Inadequate priming before startup.
9.	Motor Issues	Electrical or mechanical problems with the motor driving the pump.	<ul style="list-style-type: none">• Electrical faults (short circuits, overloads).• Motor winding failures.• Inadequate power supply or voltage fluctuations.• Overheating due to poor cooling.
10.	Hydraulic Imbalance	Imbalance in hydraulic forces causes uneven wear and vibration.	<ul style="list-style-type: none">• Impeller damage or wear.• Incorrect impeller design.• Non-uniform flow conditions.

1.5 Thesis outline

Overall, this detailed study is structured as follows:

Chapter 2. Literature Survey: It contains section 1.1 that describe the past approaches and methods for fault diagnosis, section 1.2 involved research gap and section 1.3 describe the research objective of the investigation.

Chapter 3. Experimental setup: It contains a centrifugal pump as well as sensors and valves that imitate blockages. Moreover, Sections 2.1 and 2.2 describe the process of simulation of blockage faults and their impact on the pump's performance.

Chapter 4. Blockage fault classification: there is a procedure for blockage fault classification, which consists of data collection, conversion, and structuring for further analysis with the help of machine learning. In particular, Section 3.1 examines signals using Continuous Wavelet Transform.

Chapter 5. Deep CNN Model architecture: ELUs with ReLUs are added to the InceptionV3 model for better defect detection. Section 4.1, provides a detailed explanation of the training process, including augmentation, optimization, and dropout regularisation. In Section 4.2, the procedure of hyperparameters selection is explored. Additionally, in Section 4.3, a similarity analysis of the data is conducted. In Section 4.4, the model's performance indicators are analyzed and classified into four groups, namely, precision, recall, F1 score, and accuracy. Upon that, in Section 5, the results are presented and analyzed.

Chapter 6. Result: In section 5.1, the classification of blockage faults is conducted using the InceptionV3 model. In Section 5.2, the improvements that were made are outlined. In Section 5.3, a comparison with the original InceptionV3 is conducted, and our modified model has higher accuracy and can be used for predictive maintenance in spite of a tenfold increase of computational expenses.

Chapter 7. Conclusion and Future work: Significance of the findings of this study is established and scope of future work is described.

CHAPTER – 2: Literature survey

2.1 Previous Literature

Centrifugal pumps are integral to various industries, from water treatment and agriculture to pharmaceuticals and oil and gas. Fundamentally, these pumps facilitate the movement of fluids in these industries through pipelines from one place to another by converting rotational kinetic energy into hydrodynamic energy. Despite their widespread utility, centrifugal pumps are susceptible to various faults that can significantly impair their functionality and efficiency. These faults in centrifugal pumps are broadly categorized into mechanical and hydraulic faults. Mechanical faults include bearing failures, seal leakage, imbalance, or shaft misalignment. On the other hand, hydraulic faults include cavitation, blockages, or flow recirculation [2]. These faults compromise the reliability and predictability of the pump's performance and elevate the risk of catastrophic failure, leading to significant downtime and repair costs. Thus, condition monitoring of the pump becomes vital to avoid such a situation by strengthening the maintenance technique and promoting the optimum maintenance of the pump and its components [3].

In centrifugal pump diagnostics, prior studies mainly focused on impeller cracks, bearing failure, shaft misalignment, seal defects, casing defects, and cavitation [4]. However, blockages in the pump system pipeline received very little attention, although they are among the crucial faults that impact pump performance. Blockages often result from the accumulation of foreign objects like rags, grass, or natural detritus in the foot valve or suction pipe and issues like folded pipe liners, blocked filters, or air entrainment [5]. The blockage in the pump can occur on the suction side, discharge side, or both sides of the pump and affect the pump in different ways. For instance, blockage on the suction side increases pressure drop at the impeller's eye. As the severity of this blockage increases, it causes cavitation, an increase in noise and vibration, and other significant problems like axial shaft movement and impeller shroud cracking [6]. Discharge blockage resists the fluid movement in the discharge line and initiates a backflow toward the impeller. This backflow impacts the impeller until the shaft breaks. In blockage at both suction and discharge lines, the fluid gets trapped in the casing and may explode if not noticed in time [7].

Only some studies utilized data-driven methodology to identify blockage faults in the pump. In recent study, statistical features have been extracted from vibration signals and a support vector machine (SVM) classifier was used to diagnose suction blockage faults in a pump

at different levels of severity with 86.53% success rate [5]. A comprehensive approach was proposed by combining statistical features from vibration, pressure, and motor current signals to boost the accuracy of the classifier [8]. This study achieved a maximum training and test accuracy of 93.5% and 91.8%, respectively, using pressure signals and a deep learning model. However, it is important to note the practical limitations in implementing these methodologies, especially for submersible pumps surrounded by fluid, where mounting pressure sensors, as done by [9] and [7], might not be feasible. These studies only investigated suction blockage in depth. In another study [10], vibration and motor current signals were used to look at both suction and discharge blockage faults and other mechanical faults. The data-driven methodology had recently been used to identify suction, discharge, and the simultaneous occurrence of both blockages [11]. This study focused on both suction and discharge blockage and achieves good accuracy, but it used a limited combination of these types of blockage severity.

2.2 Salient Observations and Research Gaps

Based on the above discussion, the evolution of machine learning (ML) techniques marks a significant advancement in predictive maintenance for diagnosing faults in centrifugal pumps. Initially, the studies were focused on traditional ML models like SVM and artificial neural networks (ANN) for fault detection [12]. These models rely on statistical features extracted from the time, frequency, and time-frequency domains of the acquired signals [13], [14]. However, these features often fail to capture the non-linearity associated with a system's health. Moreover, the manual selection of features requires domain expertise and sometimes leads to inappropriate choices, adversely affecting classifier performance. DNN models that can automatically extract pertinent features and lower the risk of selecting irrelevant features (Mast and Frings) address these issues [15]. However, the performance of these models largely depends on the chosen architecture, which is typically selected through trial and error, prolonging model development time [16]. This tedious process also highlights the difficulty in generalizing models for different data types, even within the same system. The generalization problem of the model is solved using the Transfer learning approach. It involves transferring knowledge from a source task to a closely related target task [17]. This approach is utilized in the study of [18], in which the Alex Net model was employed for bearing fault diagnosis on 2D time-frequency plots generated by vibration signals [19]. Similarly, a visual geometry group (VGG)16-based model was proposed for motor bearing fault diagnosis [20]. The proposed methodology converted vibration signals into RGB images and utilized a pre-trained VGG-19 model for feature extraction,

followed by a SoftMax classifier. Self-attention-based models used to find problems in rolling bearings that worked in various conditions [21]. Infrared images and pre-trained models like Inception, Xception, and Mobile Net were used to find problems in three-phase induction machines [22]. As the field progressed, these convolutional neural network (CNN) models became particularly useful in diagnosing faults in centrifugal pumps [22]. Short-time Fourier transforms (STFT), wavelet transforms, or spectrogram analyses can turn vibration or sound signals into time-frequency images. CNNs can use intricate signal patterns within images corresponding to various fault conditions, including blockages for fault classification [23]. The CNN model can extract features from images automatically by identifying edges, textures, and complex patterns specific to certain faults [23] [24]. These capabilities can also help to handle images under varying pump operating conditions, such as changes in the suction and discharge side flow areas that can alter signal characteristics [25]. These CNN models classified blockage faults by incorporating 2D images of time-frequency obtained from raw signals [8]. These pieces of literature showcase different approaches to identifying faults in the mechanical system. It mainly uses transfer learning or develops a CNN model from scratch. However, task dissimilarity between the source and target models is a crucial challenge while using transfer learning. Transfer learning relies on transferring knowledge from a pre-trained model (source task) to a new but related task (target task) [26]. However, the transferred knowledge may be less effective if the tasks are too dissimilar, leading to suboptimal performance. Additionally, selecting an appropriate pre-trained model often involves trial and error, making the process time-consuming.

Developing a CNN model from scratch requires considerable time and computational resources to train the model, especially when dealing with large datasets or complex architectures. Moreover, designing and optimizing a CNN architecture is often trial and error, which can be time-consuming and may not always yield the desired results [24].

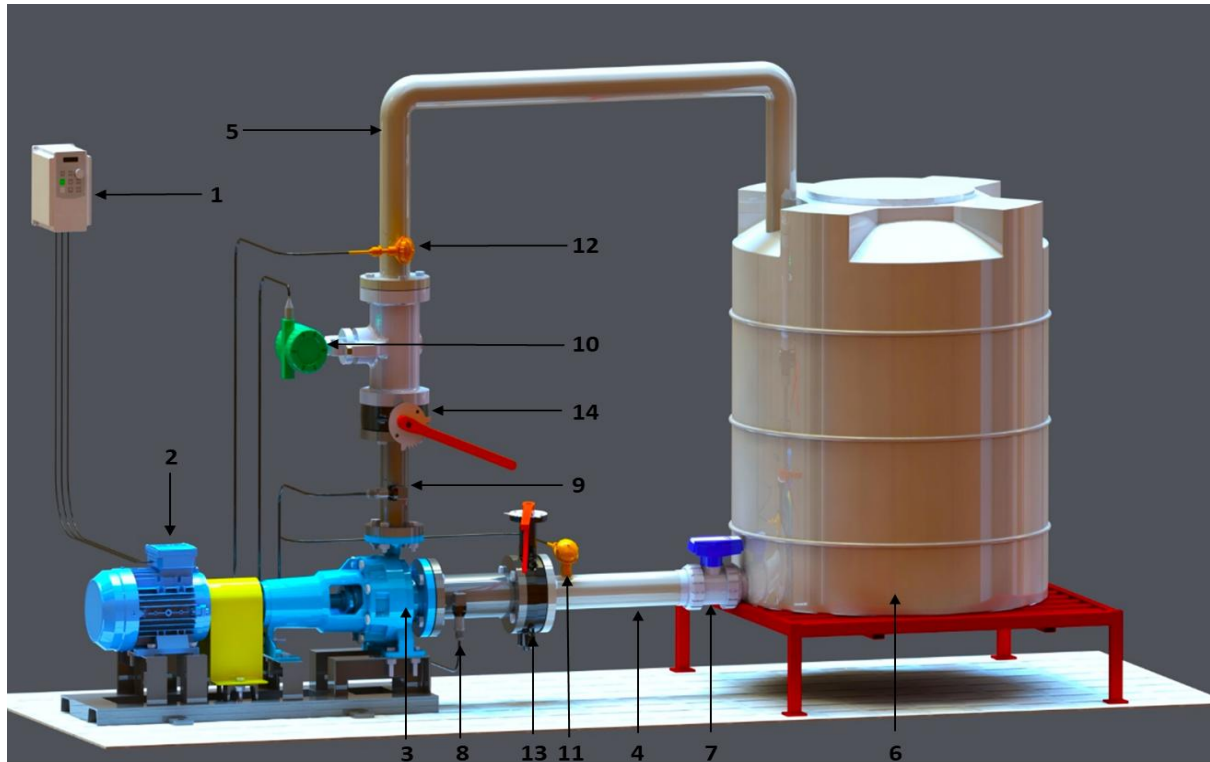
2.3 Research objective

Therefore, this study initially utilizes the architecture of the pre-trained model and further modifies it to work efficiently for the assigned task. The primary aim of this study is to develop a deep CNN model inspired by the pre-trained model - InceptionV3, that effectively identifies the blockages in the pump. Furthermore, the modified InceptionV3 will make centrifugal pumps used in many industrial settings more reliable and efficient by improving the fault diagnosis method.

CHAPTER – 3: Experimental Setup

The CAD model of the experimental facility employed to mimic blockage faults in a centrifugal pump is shown in Figure 3. A single-stage end suction centrifugal pump (Mackwell; Model: MCPP-32/160) is utilized in conjunction with a three-phase squirrel cage induction motor to power the pumping system. The pump and motor are coupled by a spider connection and mounted on an MS-fabricated base frame. A VFD (Variable Frequency Drive) (Model: VFD-S-3-030-415V) is employed to control the speed of the induction motor. In this study, water is selected as the working fluid. Water is stored in the reservoir and delivered to the pump through a suction line while the ball valve is open, ensuring continuous fluid flow. The pressurized fluid available at the discharge side of the pump is then returned to the reservoir via the discharge line. In addition, a wafer-style body-type butterfly valve with a hand lever and a fixed number of notches on the notch plate is installed into the suction and discharge lines to simulate the occurrence of any blocking problem inside the pipeline. This study focuses on three different types of blockages: suction blockage (SB), discharge blockage (DB), and suction-discharge blockage (SDB).

As illustrated in Figure 4, the notch plate on the suction side of the butterfly valves is divided into ten segments ranging from 0° in the entirely open position to 90° in the fully closed position. At the same time, the discharge side is divided into seven segments. Blockages at the suction or discharge side are simulated by gradually moving the lever toward the closing direction of the valve. A flowmeter (Scientific Devices; Model: MAG - 300/40; accuracy: 0.5%) is installed in the discharge line after the butterfly valve to record any fluctuations or variations in flow rate caused by the blockage. One absolute pressure sensor (Wika; Model: A-10; range: -1 to 1.5 bar; accuracy: 0.5%) is placed in the suction line immediately after the butterfly valve (near the pump), and the second absolute pressure sensor (Danfoss; Model: MBS 3000; range: 0 to 10 bar; accuracy: 0.25%) is placed in the discharge line just before the butterfly valve (near the pump). These sensors are linked to a data acquisition system (HYDAC; Model: HMG 4000) for measuring and acquiring data.



1. VFD, 2. Induction Motor, 3. Centrifugal Pump, 4. Suction Line, 5. Discharge Line, 6. Reservoir, 7. Ball valve, 8. Pressure Sensor – 1, 9. Pressure Sensor – 2, 10. Flowmeter, 11. Temperature Sensor – 1, 12. Temperature Sensor – 2, 13. Butterfly Valve – 1, 14. Butterfly Valve – 2

Figure 3: CAD model of the experimental facility to simulate blockage fault in a centrifugal pump, developed in the System Dynamics Lab of IIT Indore (India).

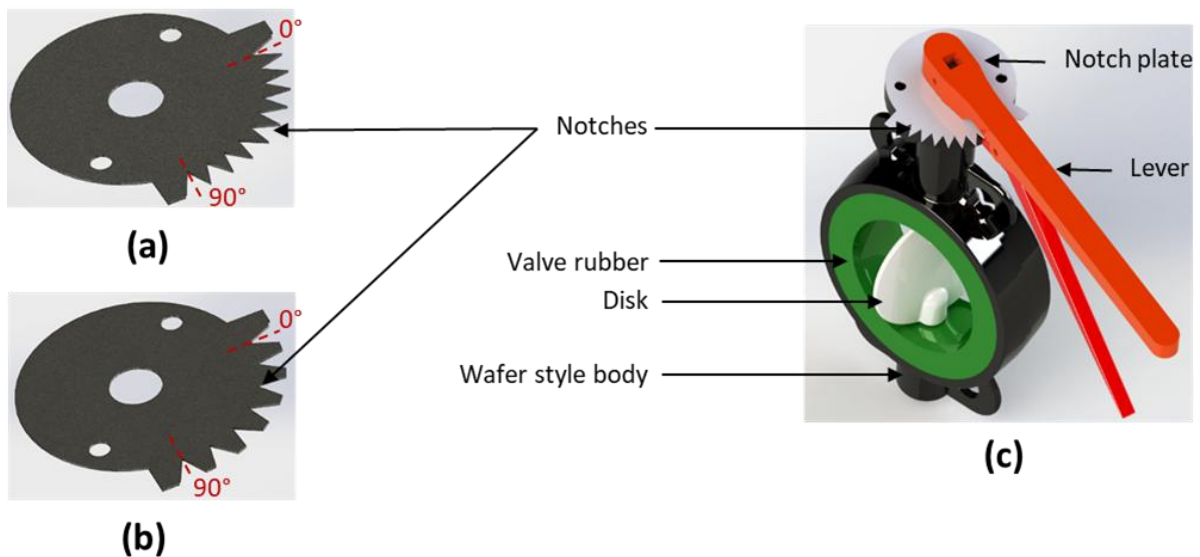


Figure 4: CAD model of (a) Notch plate with 10 notches of suction side butterfly valve, (b) Notch plate with 7 notches of discharge side butterfly valve, (c) Wafer-style body type butterfly valve.

3.1 Test procedure

This research aims to investigate the effect of SB, DB, and SDB on the performance of centrifugal pumps. Therefore, suction pressure, discharge pressure, and flow rate have been measured during tests. The tests have been performed on the pump at an operating speed of 2000 rpm. The data is acquired at a sampling rate of 10 kHz for a time span of 60 seconds. The dominant frequencies for suction and discharge pressure were observed at 100 Hz (which can be seen in CWT plots). For flow rate, the dominant frequency was perceived around 4000 Hz. To ensure that no frequency information is lost and to adhere to Nyquist's theorem, a sampling rate of 10 kHz has been chosen.

Table 2 enlists the series of pump conditions investigated in this study. A total of three distinct faults, namely suction blockage, discharge blockage, and a combination of suction and discharge blockage, are considered. The severity of these blockages is increased by increasing the notch angle. For suction blockage, butterfly valves with notch angles (degrees) of 10, 20, 30, 40, 50, and 60 block the suction line in such a way that at a 10° notch angle, only 0.8% of the flow area is blocked, whereas, at a 60° notch angle, 87.5% of the flow area is blocked in the suction line. Similarly, for discharge blockage, notches angles (degrees) of 15, 30, 45, and 60 in the discharge side butterfly valve are used to increase the discharge blockage's severity, such that a 15° notch angle blocks up to 10% of the flow area.

In contrast, a 60° notch angle blocks up to 87.5% of the flow area in the discharge line. For simultaneous occurrence of both suction and discharge blockages, a butterfly valve on the suction side is set at 10°, and the butterfly valve on the discharge side blocks the flow area by 15°, 30°, 45°, and 60°. This combination is repeated at each severity level of suction blockage until the notch angle is 60° in the suction butterfly valve. Thus, it results in 24 different combinations of simultaneous occurrences of suction-discharge blockage. Overall, 35 conditions of pumps (healthy - 1, suction blockage - 6, discharge blockage - 4, and suction-discharge blockage - 24) are included in this study.

The signals at each pump condition are acquired after the pump has attained a steady state to ensure precise and reliable data. In this case, a steady state is defined as a condition after which the mean value of flow rates does not deviate more than 0.1% of the measured flow rate for at least 30 seconds. A steady condition was attained within 30 seconds after the pump was started and after simulating the blockage fault. The signals are acquired 60 seconds later to ensure the system's stability [25].

3.2 Performance of pump

The blockage effect on the centrifugal pump can be seen with the help of performance parameters like suction pressure, discharge pressure, flow rate, head, and H-Q curve, as shown in Figure 5. A straight black dashed line on these plots compares the pump parameters in faulty condition with those in healthy condition. A notable phenomenon has been observed in centrifugal pump performance under Discharge blockage conditions (DB). When the discharge line is blocked up to DB30, there is no noticeable rise or reduction in any performance parameters of pumps shown in Figure 5.

Table 2: Details of blockage faults induced in centrifugal pump

Fault No.	Fault label	Blockage Condition	Percentage Flow Area Blocked
1	AH	At Healthy Condition (0° Blockage of both suction side (SS) and discharge side (DS) valve)	0% flow area (FA) is assumed to be blocked, ignoring the valve plate thickness
2	SB10	10° rotation of SS valve	0.8% of SS FA is blocked
3	SB20	20° rotation of SS valve	18.3% of SS FA is blocked
4	SB30	30° rotation of SS valve	40.6% of SS FA is blocked
5	SB40	40° rotation of SS valve	59.6% of SS FA is blocked
6	SB50	50° rotation of SS valve	75.5% of SS FA is blocked
7	SB60	60° rotation of SS valve	87.5% of SS FA is blocked
8	DB15	15° rotation of DS valve	10% of DS FA is blocked
9	DB30	30° rotation of DS valve	40.6% of DS FA is blocked
10	DB45	45° rotation of the DS valve	67.7% of DS FA is blocked
11	DB60	60° rotation of the DS valve	87.5% of DS FA is blocked
12	SDB1510	10° rotation of SS valve keeping 15° rotation of DS valve	0.8% on SS + 15% on DS FA is blocked
13	SDB1520	20° rotation of SS valve keeping 15° rotation of DS valve	18.3% on SS + 15% on DS FA is blocked
14	SDB1530	30° rotation of SS valve keeping 15° rotation of DS valve	40.6% on SS + 15% on DS FA is blocked
15	SDB1540	40° rotation of SS valve keeping 15° rotation of DS valve	59.6% on SS + 15% on DS FA is blocked
16	SDB1550	50° rotation of SS valve keeping 15° rotation of DS valve	75.5% on SS + 15% on DS FA is blocked
17	SDB1560	60° rotation of SS valve keeping 15° rotation of DS valve	87.5% on SS + 15% on DS FA is blocked
18	SDB3010	10° rotation of SS valve keeping 30° rotation of DS valve	0.8% on SS + 30% on DS FA is blocked
19	SDB3020	20° rotation of SS valve keeping 30° rotation of DS valve	18.3% on SS + 30% on DS FA is blocked
20	SDB3030	30° rotation of SS valve keeping 30° rotation of DS valve	40.6% on SS + 30% on DS FA is blocked
21	SDB3040	40° rotation of SS valve keeping 30° rotation of DS valve	59.6% on SS + 30% on DS FA is blocked
22	SDB3050	50° rotation of SS valve keeping 30° rotation of DS valve	75.5% on SS + 30% on DS FA is blocked
23	SDB3060	60° rotation of SS valve keeping 30° rotation of DS valve	87.5% on SS + 30% on DS FA is blocked
24	SDB4510	10° rotation of SS valve keeping 45° rotation of DS valve	0.8% on SS + 45% on DS FA is blocked
25	SDB4520	20° rotation of SS valve keeping 45° rotation of DS valve	18.3% on SS + 45% on DS FA is blocked
26	SDB4530	30° rotation of SS valve keeping 45° rotation of DS valve	40.6% on SS + 45% on DS FA is blocked
27	SDB4540	40° rotation of SS valve keeping 45° rotation of DS valve	59.6% on SS + 45% on DS FA is blocked
28	SDB4550	50° rotation of SS valve keeping 45° rotation of DS valve	75.5% on SS + 45% on DS FA is blocked
29	SDB4560	60° rotation of SS valve keeping 45° rotation of DS valve	87.5% on SS + 45% on DS FA is blocked
30	SDB6010	10° rotation of SS valve keeping 60° rotation of DS valve	0.8% on SS + 60% on DS FA is blocked
31	SDB6020	20° rotation of SS valve keeping 60° rotation of DS valve	18.3% on SS + 60% on DS FA is blocked
32	SDB6030	30° rotation of SS valve keeping 60° rotation of DS valve	40.6% on SS + 60% on DS FA is blocked
33	SDB6040	40° rotation of SS valve keeping 60° rotation of DS valve	59.6% on SS + 60% on DS FA is blocked
34	SDB6050	50° rotation of SS valve keeping 60° rotation of DS valve	75.5% on SS + 60% on DS FA is blocked
35	SDB6060	60° rotation of SS valve keeping 60° rotation of DS valve	87.5% on SS + 60% on DS FA is blocked

After DB 30, suction pressure increases with an increase in the severity level of DB as shown in Figure 5(a). The occurrence of DB increases the flow restriction in the discharge line initiating a backflow towards the suction side (low-pressure zone) that ultimately increases the suction side pressure. The restriction offered in the discharge line also increases the pressure in the discharge line, as shown in Figure 5(b). The pump is operating at a constant speed regardless of the pump's condition, whereas the flow of the pump reduces due to blockage, as shown in Figure 5(c). It leads to an increase in the head of the pump (as shown in Figure 5(d)) which increases the discharge pressure as suction pressure is already high due to backflow.

Whereas in the case of SB, suction pressure at the exit of the suction line decreases with an increase in suction blockage severity level, as shown in Figure 5(a). This pressure drops due to an increase in flow resistance that occurs due to reduced cross-section of suction flow with increased severity of SB. The reduced suction pressure increases the pump's work to attain the desired head, ultimately leading to a drop in discharge pressure, as shown in Figure 5(b). The total head of the pump increases as the flow rate of the pump is reduced due to the occurrence of blockage whereas the pump rotates at a constant speed, as shown in Figure 5(d). It is depicted in Figure 5(e) that whenever the flow rate decreases then it leads to an increase in the head of the pump.

In the case of combined blockage (SDB), the effect of both DB and SB is working together. In all conditions, as shown in Figure 5, SDB15 and SDB30 follow the same trends as SB with almost the same intensity. In the case of SDB45, it follows almost the same trend as SB with a higher intensity as the severity level of DB has also increased, so at the initial level, only the suction pressure and discharge pressure increased based on DB 45. Afterward, it changes with the severity of SB. It also shows the dominance of suction side blockage over the discharge side. Meanwhile, in the case of SDB60, it follows the trend of the DB as the severity of DB is highest, and thus, DB is completely dominating in this case, and the effect of SB is almost minimal.

Parameter for assessing the severity of blockages in centrifugal pumps, directly impacting pump performance. It presents a clear, consistent trend when responding to varying blockage conditions, a trend that is crucial for the predictive analytics of machine learning algorithms. As suction pressure intricately affects the pump's head and flow rate, its fluctuations offer a dependable measure of its operational state. Also, from the above analysis, SB fault is the dominating one, so the parameter close to it can provide a clear picture of pump performance. Here, the closest parameter is suction pressure. This consistent and measurable response to blockages makes suction pressure an ideal parameter for monitoring and predicting pump performance, facilitating the early detection and classification of faults in pump systems.

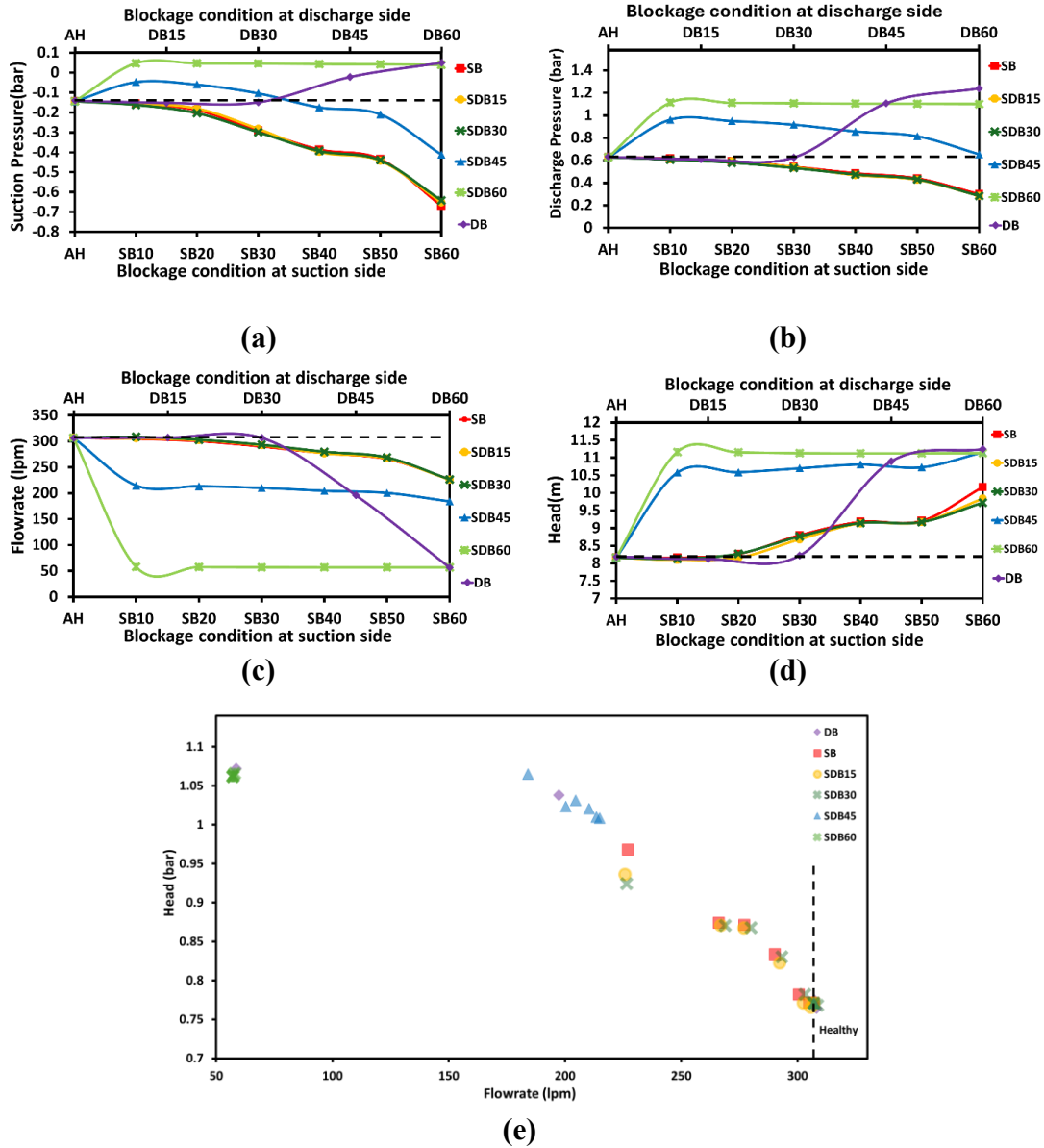


Figure 5: Pump performance parameter (a) Suction Pressure, (b) Discharge Pressure, (c) Flowrate, (d) Head, (e) Head vs Flowrate (H-Q) curve. (For each plot, mean values of parameters are taken). Notation: SDB1510 means the SDB15 curve at SB10 in the plots.

From the above observation, suction pressure is critical. Although instructive, the performance curves of centrifugal pumps only partially capture the complex interaction of variables such as flow rate, pressure, and temperature when there is a blockage. These curves are only capable of visual trend analysis and cannot uncover the intricate, non-linear connections that machine learning algorithms are highly skilled at deciphering. Graphs are inadequate in predictive analytics and measuring uncertainty, which is essential for the maintenance department. Machine learning offers a reliable and scalable solution that delivers objective and automatic fault categorization, which is crucial for maintenance in the modern pump industry.

CHAPTER – 4: Blockage faults classification

4.1 Classification methodology

The research methodology encompasses a comprehensive flow, as shown in Figure 6, starting with data acquisition from a pump test rig, utilizing a pressure sensor in conjunction with a HYDAC system. The collected data is then seamlessly transferred to a computer for further processing. In the subsequent step, the acquired data is converted from the default extension (.herf4) to a .csv format, a widely accepted format for handling and analyzing large data. Further pre-processing is carried out on the MATLAB platform. Data is first filtered to precise 1-second intervals to refine it for relevant features. Following the filtration, the .csv files are meticulously organized into folders categorized by their respective classes, same as the fault labels shown in Table 2. Further, the images and labels derived from the CWT are converted into NumPy arrays, the standard numerical representation in Python, paving the way for machine learning applications. The complete dataset is divided into three sets: training,

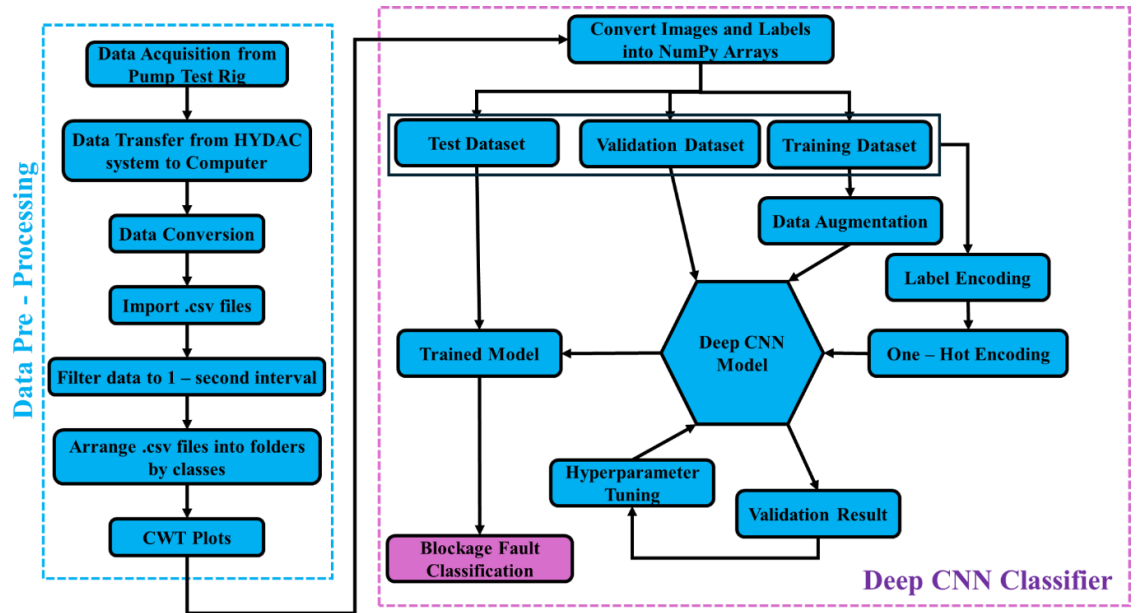


Figure 6: Methodology adopted for blockage fault classification in a centrifugal pump.

validation, and testing dataset. These datasets are integral for the development of a robust predictive model. Techniques such as image transformations are applied to augment the training data, enhancing the model's ability to generalize from the data. Concurrently, the class labels undergo encoding—initially through label encoding to translate categorical labels into a numerical format, followed by one-hot encoding to transform these numerical labels into binary vectors conducive to neural network training. A Deep Convolutional Neural Network (CNN)

is at the heart of model development and is trained on the augmented and encoded dataset.

The trained model is fine-tuned using a hyperband hyperparameter optimization method, which uses the validation results and targets the best performance possible. The outcome of the entire activity is the use of the trained and fine-tuned model to classify blockage faults, which demonstrates the model's ability to predict and diagnose faults in new data. A further analysis by the author reveals a systematic study involving mechanically related systems and data analytics systems, presenting an innovative step towards predictive maintenance in pump systems.

4.2 Continuous Wavelet Transform

The CWT is a critical signal processing tool, which is very good at capturing the different frequency components of a non-stationary signal. These wavelets are instrumental as they are localized in both the time and frequency domains [26]. CWT provides better Time-Frequency resolution than EMD, VMD, EEMD etc.[27]

This localization allows for a more complex and accurate decomposition of a signal. CWT functions by continuously breaking down a signal across various scales and positions, a process mathematically expressed as [28]

$$CWT(\tau, s) = \frac{1}{\sqrt{|s|}} \int x(t) \psi^* \left(\frac{t - \tau}{s} \right) dt \quad (1)$$

here, $\psi(t)$ symbolizes the mother wavelet, with τ and s representing the translation and scale parameters, respectively. The Morse wavelet known for its symmetry and smoothness, is often utilized in CWT [28], [29]. Characterized by its unique formula,

$$\psi(t) = e^{-(b^t)} e^{i\omega_0 t} \quad (2)$$

Morse wavelet is used as it can be tailored to specific data characteristics through its adjustable parameters b and ω_0 . Though default values of $b = 3$, $\omega_0 = 60$ are taken here as it gives a good balance between time and frequency resolution for suction pressure signals in MATLAB [30]. Thus, CWT, especially with Morse wavelets, offers superior time-frequency localization, which is essential for analyzing signals with transient features. The scalogram is the output of CWT and illustrates the contribution of each frequency band to a signal's energy over time. It is particularly beneficial for better time localization for short-duration,

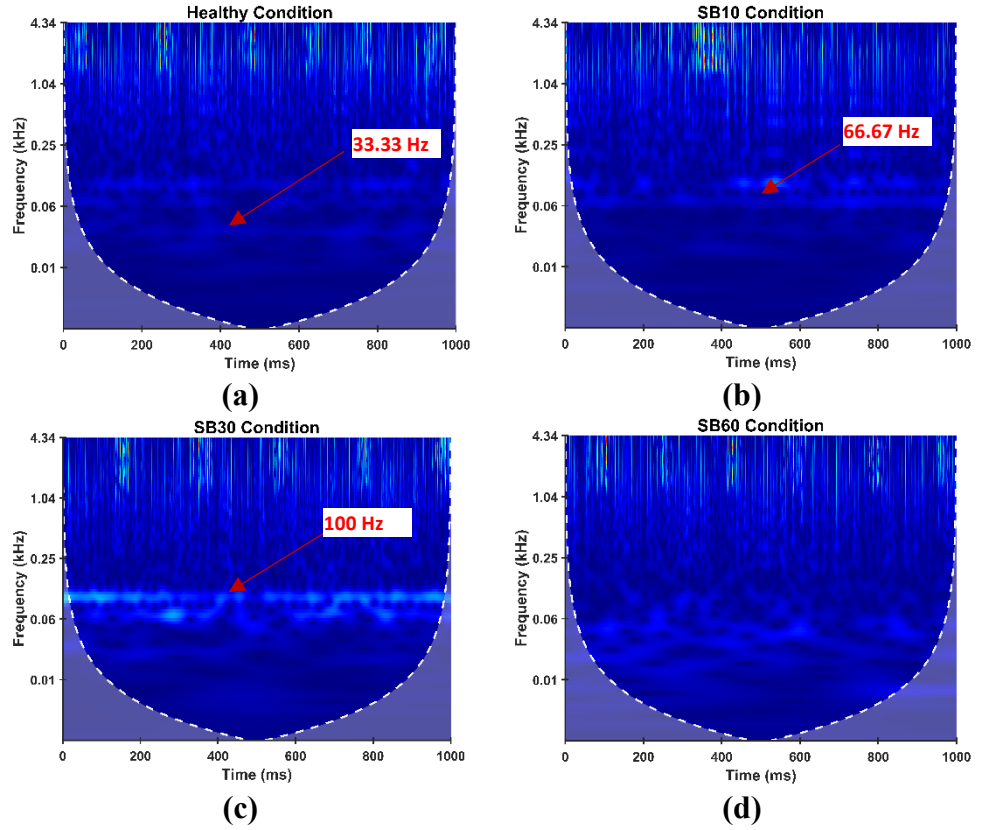


Figure 7: CWT of suction pressure signals (a) Healthy condition and severity level of suction blockage namely (b) SB10, (c) SB30, and (d) SB60.

high-frequency events and improved frequency localization for long-duration, low-frequency events.

CWT is employed to conduct an in-depth frequency analysis of the suction pressure signals. These signals are often characterized by their complex and dynamic nature. It is essential to explore the frequencies present in the signals over time to understand the underlying behavior of pumps. The pump's rotational frequency is 33.33 Hz, and as the pump rotates at 2000 rpm, a dimly visible band can be seen in Figure 7(a). The first harmonic of rotational frequency is 66.67 Hz, and a band around this frequency can be seen in the CWT plots in Figure 7(b), representing the force dynamics working in a centrifugal pump [31]. A dominant frequency of 100 Hz is present in almost all blockage conditions (Figs. 7 to 12). The second harmonic of the fundamental frequency has arisen due to vibration caused by a hydraulic imbalance between the pump casing and impeller and the complex turbulent nature of the fluid due to blockages. A frequency of 233.31 Hz can be seen in Figure 6a, denoting the blade passing frequency as the number of impeller vanes is seven in the considered pump. Generating CWT plots

enables the visual inspection and analysis of different frequencies manifested throughout the signal.

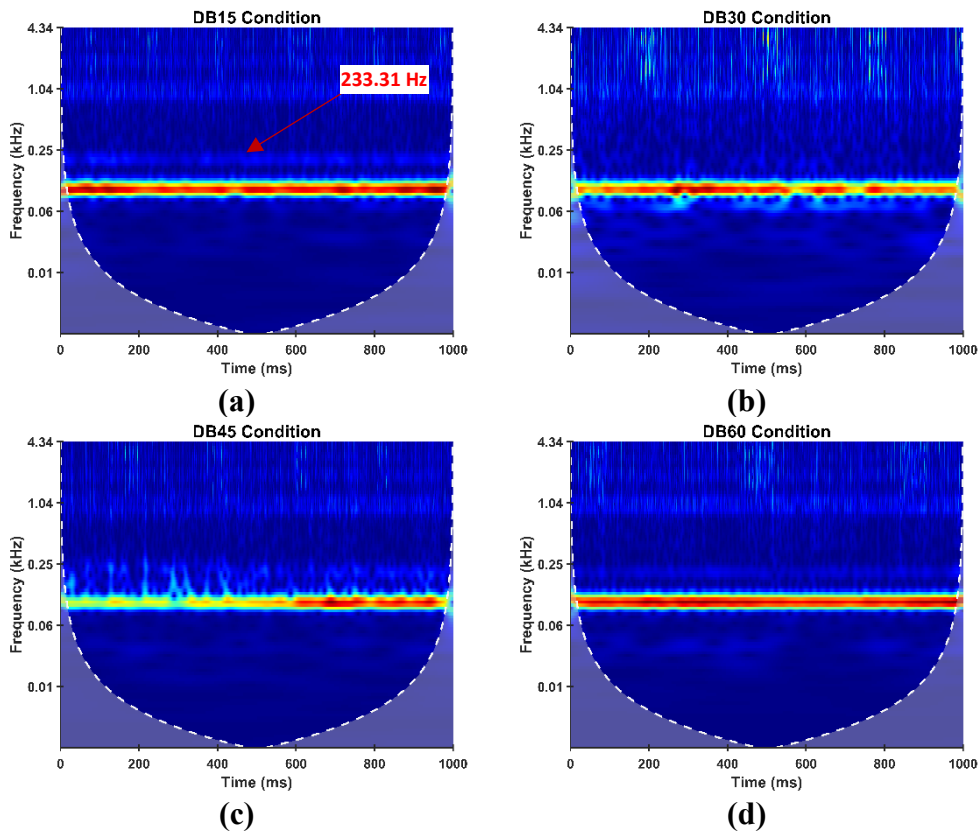


Figure 8: CWT of suction pressure signals at different severity levels of discharge blockages, namely (a) DB15, (b) DB30, (c) DB45, and (d) DB60.

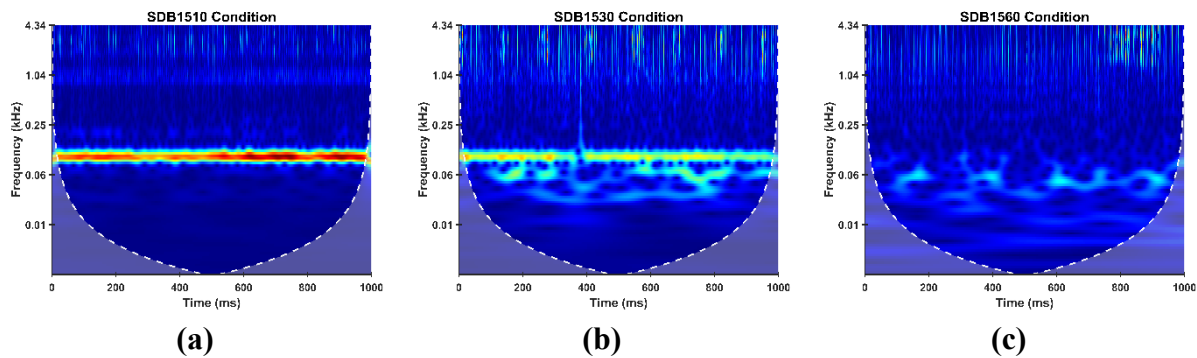


Figure 9: CWT of suction pressure signals at different severity levels of discharge blockages, namely (a) SDB1510, (b) SDB1530, and (c) SDB1560.

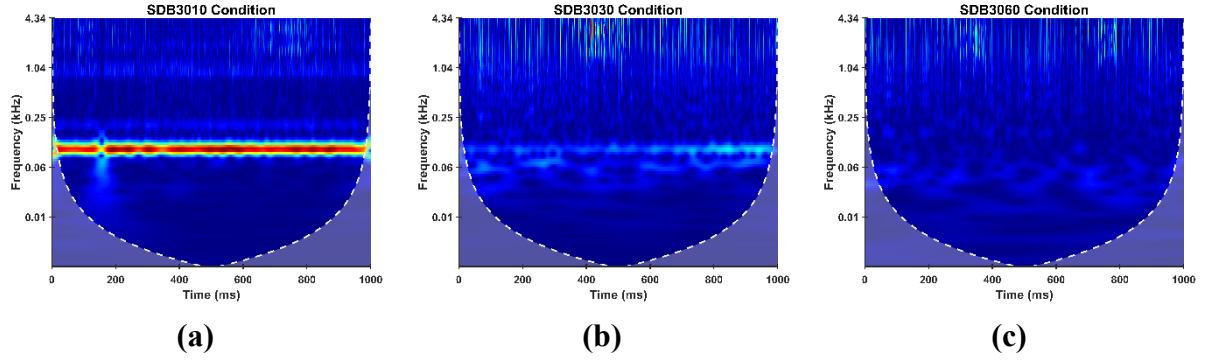


Figure 10: CWT of suction pressure signals at different severity levels of discharge blockages, namely (a) SDB3010, (b) SDB3030, and (c) SDB3060.

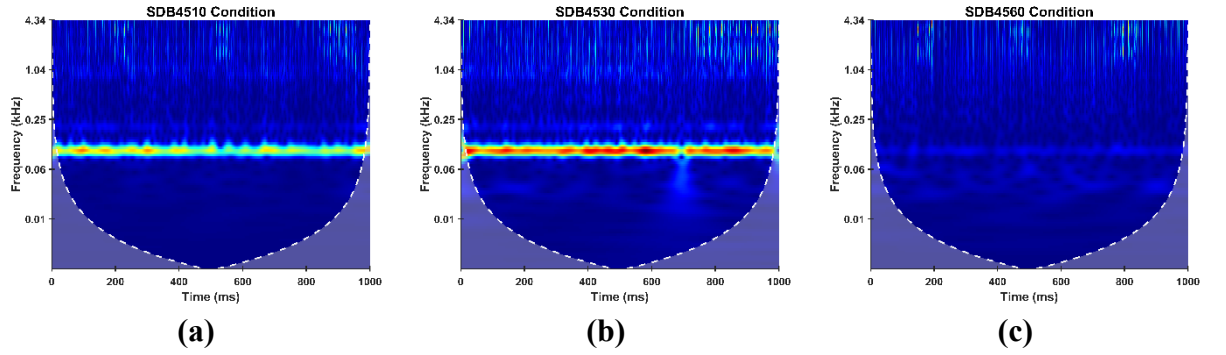


Figure 11: CWT of suction pressure signals at different severity levels of discharge blockages, namely (a) SDB4510, (b) SDB4530, and (c) SDB4560.

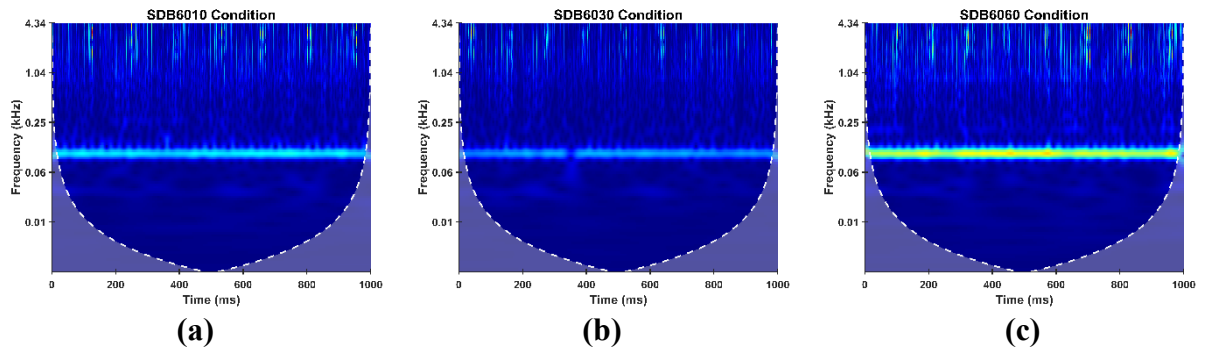


Figure 12: CWT of suction pressure signals at different severity levels of discharge blockages, namely (a) SDB6010, (b) SDB6030, and (c) SDB6060.

Despite these advantages, CWT does introduce practical constraints: generating a full scalogram for each sample requires roughly two minutes on our workstation, which challenges real-time monitoring.

Furthermore, while CWT excels at highlighting fault-related spectral content, its effectiveness diminishes when the signal-to-noise ratio drops below ~ 10 dB or when pressure fluctuations are of very low amplitude—even though our test rig data maintained an SNR above 20 dB, field deployments may require additional pre-filtering or adaptive thresholding [32] [33]. To address these limitations, future work will explore faster CWT implementations (e.g., wavelet packet transforms), scale-selection heuristics to reduce computation, and hardware-in-the-loop prototyping to benchmark real-time feasibility.

In this study, suction pressure data is prepared for classification using deep convolutional neural networks (CNNs), as it does not need manual feature extraction. CNNs are renowned for their ability to extract features from data with a grid-like or spatial structure [34], [35]. However, suction pressure signals are inherently one-dimensional time series data that do not naturally align with the grid-like input format expected by CNNs. To overcome this challenge, CWT is leveraged to transform the one-dimensional pressure signals into two-dimensional CWT images (scalograms). These images effectively represent the time-frequency features of the signals across different scales. This transformation allows us to adapt the data into a format suitable for CNN analysis. Consequently, CNNs could harness their capabilities to capture spatial relationships and features within the suction pressure data [36]. This approach enhanced the data's utility for classifying blockages in centrifugal pumps.

CHAPTER – 5: Deep CNN Model architecture

The advent of deep convolutional neural networks has precipitated a series of breakthroughs in image recognition. Among the diverse array of architectures, InceptionV3 has distinguished itself as a model of choice, striking a fine balance between computational efficiency and depth of structure. This delicate equilibrium allows it to discern complex patterns in image data [37]. The decision to employ InceptionV3, depicted in Figure 13(a) as the scaffold for this investigation, was driven by its exemplary performance on a broad spectrum of image recognition tasks, including the analysis of Continuous Wavelet Transform (CWT) plots, which are complex.

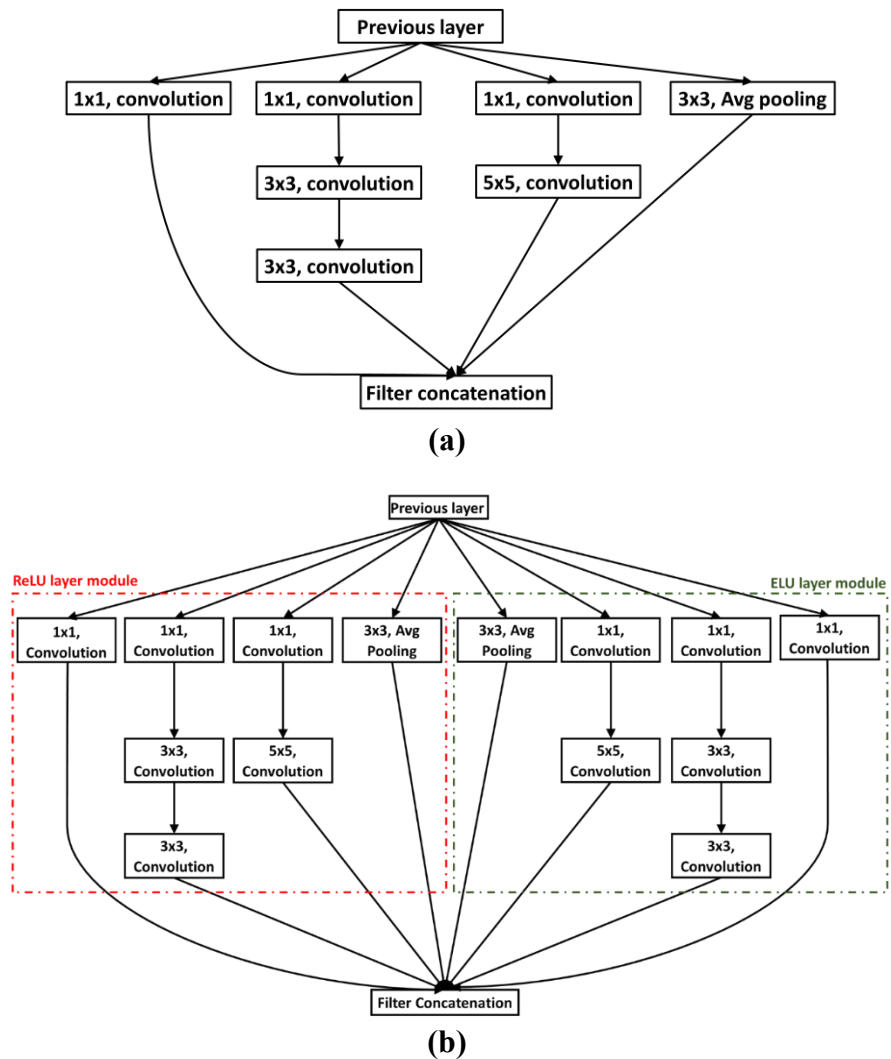


Figure 13: Basic module of (a) InceptionV3, (b) Modified InceptionV3.

However, this study aims to push the boundaries of fault detection in centrifugal pumps, revealing the limitations of InceptionV3, particularly in identifying the subtle features indicative of incipient malfunctions. This recognition of InceptionV3's untapped potential to detect early fault

signatures catalyzed the modification efforts. A postulation was made that introducing Exponential Linear Units (ELUs) alongside the conventional Rectified Linear Units (ReLUs) could enrich the model's feature extraction capabilities. To materialize this concept, in parallel, an ELU layer is introduced in the module that mirrors the structure of the ReLU layer module, depicted in Figure 13(b). However, it replaces ReLU with the ELU activation function, which particularly captures non-linearities and normalizes the activations to a zero mean, thereby mitigating the vanishing gradient problem [38]. This hybrid approach is designed to amalgamate the benefits of both ReLU and ELU activations within a unified framework. By doing so, the network can leverage the rapid learning characteristics and positive domain specialization of the ReLU while simultaneously harnessing the ELU's ability to process negative activations more effectively, which leads to richer feature maps and improved generalization.

The integration of ELU also contributes to a more consistent gradient flow during backpropagation, which is hypothesized to enhance the learning process and yield performance gains on many recognition tasks. The proposed architecture, therefore, stands as a sophisticated evolution of the InceptionV3 Net, aiming to provide a more comprehensive understanding and a more refined feature extraction mechanism within deep convolutional neural networks. Therefore, the present research puts forth a customized Convolutional Neural Network architecture keeping inceptionV3 as the base towards better classification of blockage faults in centrifugal pumps. The novel model is implemented using TensorFlow and Keras libraries and represents the perfect fusion of depth and complexity to grasp the feature describing the fault detection process of image-based faults[39].

Two major custom functions are used for building the convolution layers: `conv2d_bn` and `conv2d_bn1`. Both of them build a convolutional layer and then build a batch normalization and activation layer. The function `conv2d_bn` uses the ReLU activation function, while `conv2d_bn1` uses ELU. The combination of these two activation functions is strategically chosen; ReLU is easy to consider, while the ELU avoids the vanishing gradient problem. Most importantly, the Glorot weight initializer in these layers helps in keeping the variance of inputs, making the training dynamics more efficient. In the beginning, the model is initialized with an input layer designed to ingest the images of centrifugal pumps (image height = 312, image width = 312, no. of channels = 3). Following this, two primary blocks of convolutional layers process the input images through multiple convolutional stages, each varying in filter sizes and strides. The incorporation of MaxPooling2D layers in these blocks serves to reduce the spatial dimensions, emphasizing significant features while reducing computational complexity. In the proposed model, architecture like InceptionV3-like modules is named from concatenated-1 to concatenated-15. These modules are designed to capture diverse features by paralleling multiple convolutional branches with varying

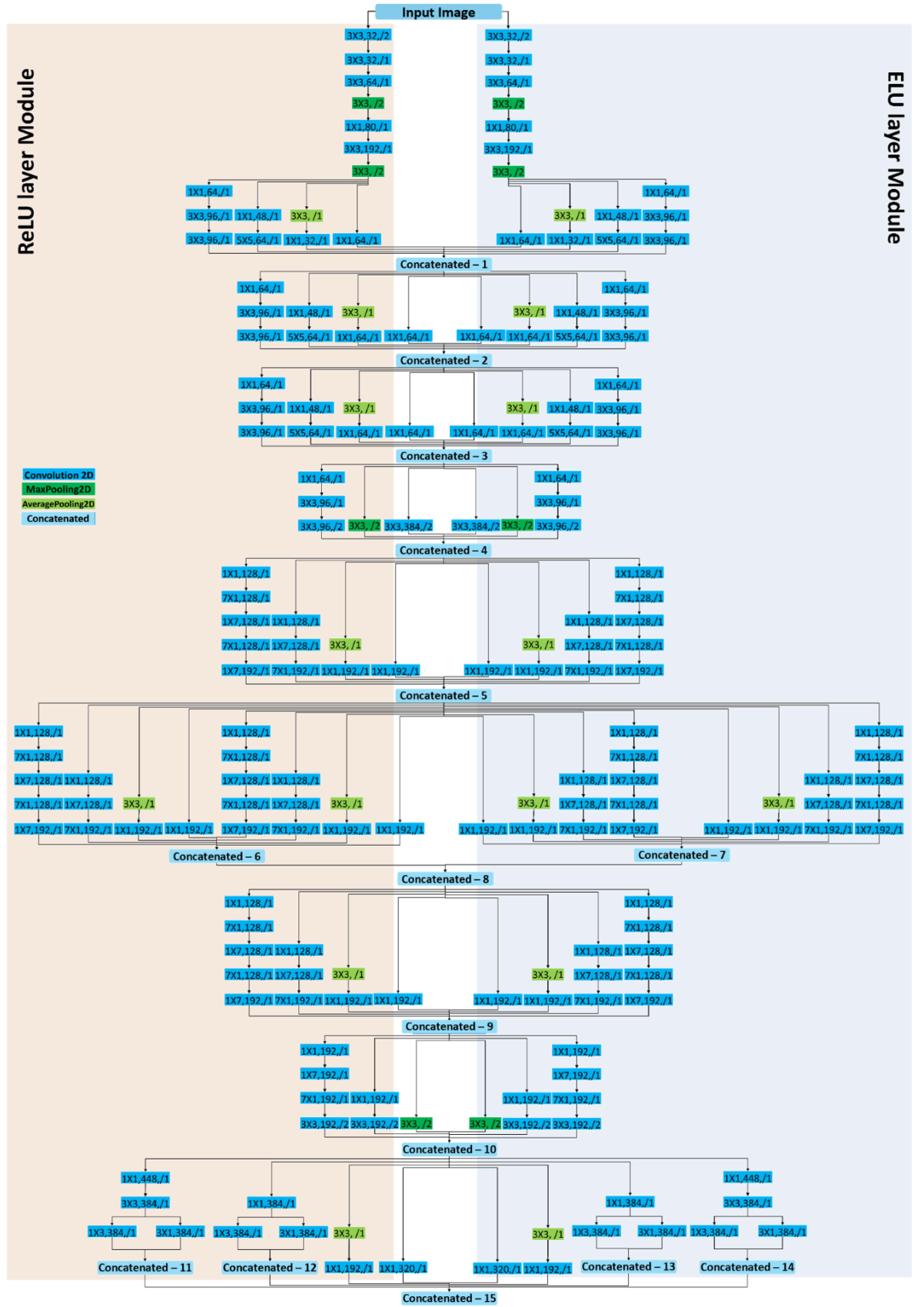


Figure 14: Modified InceptionV3 network with no. of kernel and size of kernel. Here, only ReLU layer Module can be consider as InceptionV3 network.

filter sizes, as shown in Figure 14. This multi-scale processing allows the network to learn granular and abstract representations for accurately identifying blockage faults in centrifugal pumps. The outputs of these branches are concatenated, forming rich and comprehensive feature maps.

5.1 Training Methodology

In this study, the training methodology of the modified InceptionV3 Deep CNN model was meticulously crafted to ensure robust classification of blockage faults in centrifugal pumps. The data augmentation process was pivotal, employing the ImageDataGenerator to expand our training dataset's diversity artificially. This process included a rotation range of 10 degrees, a width and height shift range of 20%, a shear range of 20%, a zoom range of 20%, and applying horizontal flips. These transformations, carefully selected based on their relevance to the real-world variability of pump operation conditions, enabled the model to learn from a more representative set of potential blockage scenarios. To optimize the learning process, ReduceLROnPlateau callback is incorporated, which meticulously monitored the validation loss, reducing the learning rate by 20% when no improvement was seen after five epochs. This adaptive learning rate approach, complemented by a verbose feedback mechanism and a lower bound learning rate of $1e-6$, allowed for fine-tuning of the model's convergence, preventing overshooting, and facilitating the navigation of the loss landscape more effectively. Regularization is introduced through two dropout layers within the dense sections of the purpose network, as depicted in Figure 15, with a rate of 70% and 50%, to prevent overfitting by

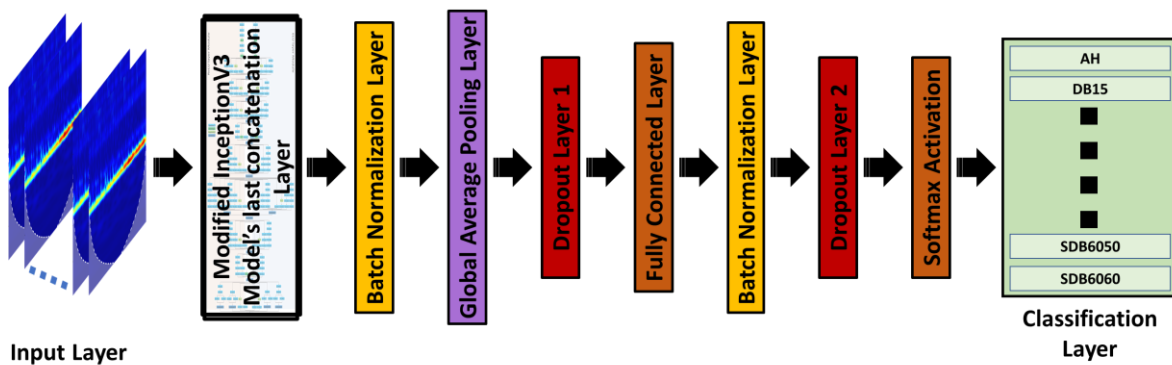


Figure 15: Complete layout of Modified InceptionV3 model-based classifier.

randomly omitting neuron units during training. This choice results from extensive experimentation, optimizing the balance between learning capacity and generalization.

The training was executed over 50 epochs with a batch size of 32, which was determined to be the optimal balance between

computational efficiency and model performance. With a patience of 10 epochs, the early stopping mechanism ensured that training ceased promptly if the validation loss stagnated, thereby preserving the best-performing model state and avoiding overfitting. On the base level, this data augmentation strategy, combined with dynamic learning rate, early stopping, and dropout regularization, contributed toward making a robust model. This holistic approach has created such an environment that produced good learning. It is thus precluding the training from the common pitfalls like overfitting, which is associated with Deep Learning Training, making the model reliable and valid for use in practical applications post-completion of training. After training, the model is evaluated on a test dataset. High accuracy was achieved, and the results were comprehensively traced using a CSV logger. Finally trained models are saved in .h5 format, so that our research findings are also reproducible through this script and the model can be easily deployed for further validation or operational use.

In this study, a robust and precise approach for classification of the blockage faults in the centrifugal pump is employed. The developed modified inceptionV3 Deep CNN model run over a strong computational set-up with a 12th Gen Intel(R) Core (TM) i9-12900 processor, 64 GB RAM, and a 16 GB Nvidia A4000 GPU. The dataset, comprising diverse fault conditions and a healthy state, was meticulously split into training, validation, and test sets, ensuring a comprehensive representation of each class. Further, sklearn's `train_test_split` with stratification is utilized to maintain uniform class distribution across these sets. In this study, on Hyperband hyperparameter tuning the best Training:Validation:Test ratio is obtained as 70:15:15 as shown in Table 2, which means 5880 samples for training, 1260 for validation, and 1260 for testing (36 data for every 35 classes).

5.2 Hyperparameter selection

Hyperparameters are the parameters of the learning algorithm itself, which need to be set before the learning process begins. These are not learned from the data but determine the learning process's efficiency and effectiveness. Selecting the correct hyperparameters can be the difference between an average model and a highly accurate one [11].

- i. **Dropout Rate:** Dropout is a regularization technique that randomly sets a fraction of input units to 0 at each update during training, which helps in preventing overfitting. This paper uses two dropout layers: one after the Global Average pooling layer (Dropout 1) and the second just before the last dense layer (Dropout 2) as a part of its architecture. Adjusting these rates impacts the network's ability to learn shared patterns and generalize better.

- ii. **Learning Rate:** The learning rate controls the adjustment of the weights in the network concerning the loss gradient. If the learning rate is too high, it might prevent the model from converging too quickly to a suboptimal solution, while a too-low rate might stall the training process.
- iii. **Batch Size:** The batch size determines the number of samples propagated through the network before the weights are updated. Smaller batches mean the gradient estimation is less accurate and the computation is fast. Larger batches provide a more accurate estimate of the gradient but are computationally heavier.
- iv. **Learning Rate Reduction (Factor and Patience):** This relates to reducing the learning rate once the learning stagnates, which is implemented via the ReduceLROnPlateau callback. The factor defines the rate by which the learning rate is reduced, and patience specifies the number of epochs with no improvement, after which the learning rate will be reduced.

Keras Tuner is a library that helps to pick the optimal set of hyperparameters for the TensorFlow program. In hyperband hyperparameter optimization, the goal is to discover the set of hyperparameters that optimizes a given objective function (here, validation loss) under a fixed resource constraint (computational budget) [40]. Traditional grid or random search strategies need to consider resource allocation, often leading to inefficient exploration of the hyperparameter space. It operates under the principle of adaptive resource allocation to configurations based on their performance. It starts by evaluating many configurations with a few resources and iteratively focuses on the most promising ones by allocating them more resources.

Table 3: Selection of split ratio (Training: Validation: Test) for modified inceptionV3 model based on hyperparameter tuning.

S.N.	Training: Validation: Test	Dropout rate1	Dropout rate2	Factor	Patience	Learning rate	Batch size	Validation accuracy
1	54:23:23	0.3	0.7	0.7	1	0.000001	16	81.93
2	60:20:20	0.1	0.4	0.6	1	0.0001	8	88.89
3	64:18:18	0.5	0.4	0.1	10	0.001	64	92.39
4	70:15:15	0.7	0.5	0.2	5	0.001	32	94.05
5	74:13:13	0.1	0.1	0.1	5	0.000001	8	93.15
6	80:10:10	0.1	0.6	0.9	2	0.0001	8	91.73

Table 4: Hyperparameter tuning in Modified InceptionV3 model.

S.N.	Dropout 1	Dropout 2	Learning rate	Batch size	factor	patience	Validation loss
1	0.7	0.3	0.000322778	256	0.2	9	0.629793584
2	0.3	0.1	0.001071194	128	0.2	7	0.627495348
3	0.9	0.9	0.000324678	32	0.3	5	0.622682214
4	0.1	0.3	7.46136E-05	32	0.5	7	0.612150788
5	0.3	0.3	6.84943E-05	64	0.4	5	0.611100435
6	0.1	0.3	3.60859E-05	16	0.1	7	0.610841513
7	0.3	0.3	0.000181215	32	0.2	7	0.610553682
8	0.5	0.1	7.3081E-06	32	0.2	7	0.610186636
9	0.7	0.1	0.000275012	16	0.5	1	0.609982133
10	0.7	0.3	0.000508198	256	0.1	5	0.609859705
11	0.5	0.1	8.18456E-06	32	0.3	1	0.606808126
12	0.3	0.1	3.44519E-05	16	0.1	7	0.606670082
13	0.3	0.1	0.001071194	128	0.2	7	0.604586959
14	0.3	0.1	0.00077409	32	0.1	9	0.603549957
15	0.7	0.3	0.004667584	128	0.1	5	0.596106768
16	0.5	0.1	0.000116265	128	0.1	7	0.592809558
17	0.5	0.3	0.000104122	16	0.1	5	0.591723323
18	0.1	0.3	0.001257702	16	0.2	3	0.591240227
19	0.3	0.3	6.84943E-05	64	0.4	5	0.589580119
20	0.7	0.3	4.68405E-05	16	0.4	3	0.568948269
21	0.9	0.7	0.000750392	64	0.1	1	0.565923870
22	0.3	0.3	0.000181215	32	0.2	7	0.565638244
23	0.5	0.5	0.000616669	16	0.5	9	0.557937324
24	0.3	0.3	0.000147181	32	0.5	3	0.554159284
25	0.5	0.7	0.000223536	16	0.5	1	0.553131044
26	0.5	0.9	0.000201148	16	0.4	1	0.550927758
27	0.7	0.7	0.000147209	64	0.4	1	0.547474086
28	0.9	0.3	0.001764999	16	0.5	5	0.545052648
29	0.7	0.1	0.000172047	128	0.3	9	0.537416518
30	0.7	0.1	0.000275012	16	0.5	1	0.534935713
31	0.7	0.3	0.001715325	128	0.2	5	0.530338645
32	0.7	0.9	0.002871743	128	0.3	5	0.505925477
33	0.9	0.7	0.000477262	64	0.4	9	0.497304231
34	0.3	0.7	0.000325916	16	0.2	5	0.497002602
35	0.5	0.7	0.000469921	128	0.1	7	0.492869943
36	0.9	0.5	8.64884E-05	256	0.4	3	0.492532194
37	0.1	0.3	0.001257702	16	0.2	3	0.472507685
38	0.7	0.3	0.000508198	256	0.1	5	0.470612168
39	0.5	0.7	0.001212391	256	0.2	1	0.456039131
40	0.1	0.7	0.001299906	64	0.3	3	0.453462929
41	0.9	0.3	0.001764999	16	0.5	5	0.442794502
42	0.9	0.3	0.000108393	256	0.2	9	0.433838964
43	0.1	0.9	0.000755961	64	0.5	7	0.422949404
44	0.9	0.5	0.001190941	32	0.2	5	0.394790471
45	0.9	0.7	0.000750392	64	0.1	1	0.393366039
46	0.9	0.5	0.000453812	64	0.1	3	0.328925043
47	0.7	0.5	0.000302548	16	0.3	5	0.304232627
48	0.7	0.5	0.000275863	32	0.2	1	0.292185843
49	0.5	0.7	0.000862544	32	0.3	7	0.276416749
50	0.7	0.5	0.001004100	32	0.2	5	0.182022452

The modified InceptionV3 model is tuned with the following values of hyperparameters: Dropout rate {0.1, 0.3, 0.5, 0.7, 0.9} for both Dropout 1 and Dropout 2, Learning rate { 1e-2, 1e-3, 1e-4, 1e-5, 1e-6 }, Batch size {16, 32, 64, 128, 256}, factor { 0.1, 0.2, 0.3, 0.4, 0.5 }, patience {1, 3, 5, 7, 9}. In this case, the best 50 lowest validation loss results are shown in Table 3 after many iterations. Thus, the optimal values of hyperparameters are Dropout 1 = 0.5, Dropout 2 = 0.5, Learning rate - 1e-2, Batch size - 32, factor = 0.2, patience 5.

5.3 Dataset similarity analysis

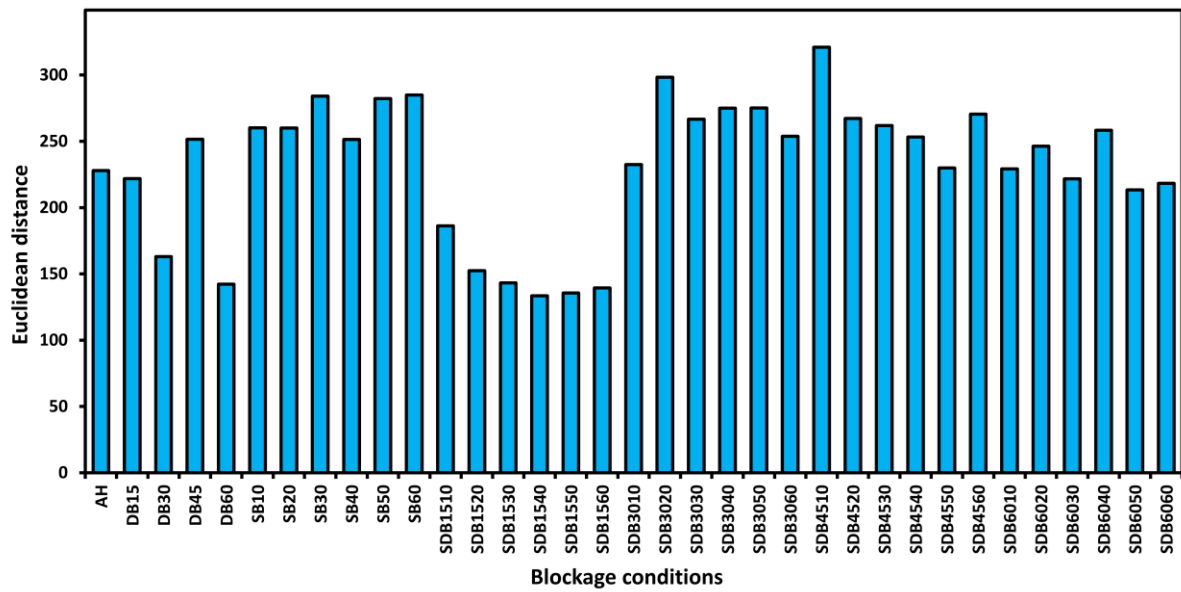


Figure 16: Euclidean Distance measures the dissimilarity between the training and test images. Higher values indicate greater dissimilarity.

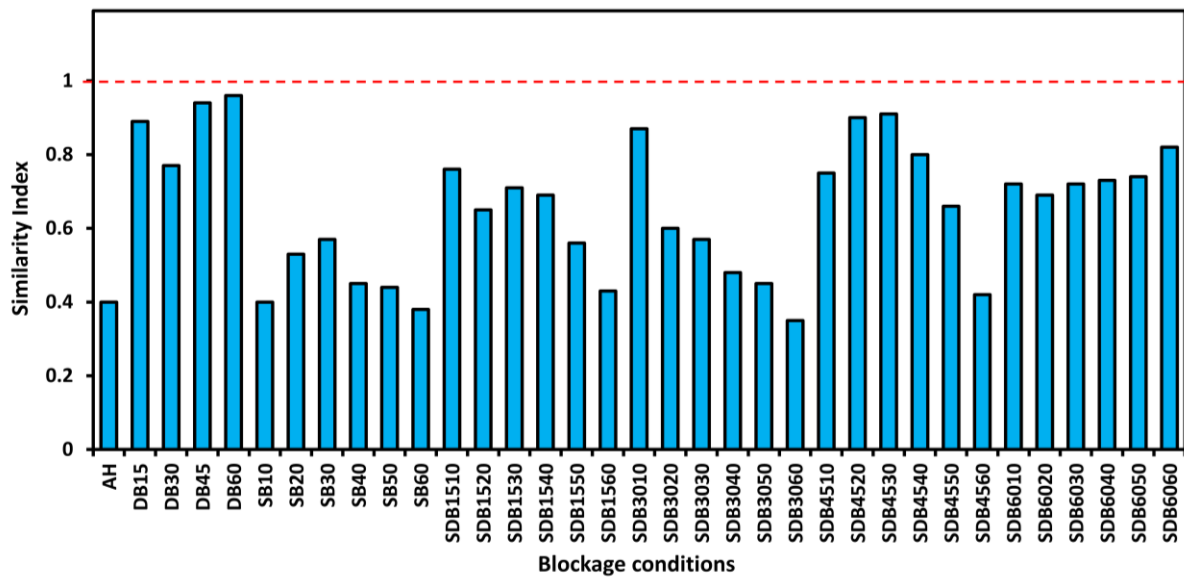


Figure 17: Universal Quality Index (UQI) measures the similarity between the training and test images. Values close to 1 indicate high similarity, while values near 0 indicate low similarity.

Since the image dataset for training and testing is from the same specimen, it is crucial to evaluate the differences between the training and test datasets. To improve the model's generalization and efficiency, the training dataset should differ slightly from the test dataset. In this study, the similarity between training and test images has been examined using Euclidean distance and Universal Quality Index (UQI) metrics. Euclidean Distance was selected as it measures the straight-line difference between corresponding pixels, providing a quantitative

measure of dissimilarity, and UQI for its ability to model image distortion based on correlation, luminance, and contrast, giving a comprehensive similarity index [42, 43]. In the Euclidean distance plot (Figure 16), significant variability between the training and test datasets is indicated by data moving away from the zero line. In the UQI plot (Figure 17), the data below the red dashed line at 1 shows a degree of dissimilarity. Both plots demonstrate that for all classes of faults, the training and test datasets are slightly different. This variability confirms that the introduced data augmentation technique provides a range of differences, validating the robustness and generalization capability of the Modified InceptionV3 model. Since the data should not be overly altered to avoid issues with InceptionV3 model training, further alteration is unnecessary. This analysis supports the model's effectiveness in handling diverse conditions, as reflected in the test data.

5.4 Model performance evaluation

Evaluating the proposed model for classifying blockage faults in centrifugal pumps is essential. The confusion matrix contained comprehensive information on the model's performance, showcasing the correct and incorrect predictions in a heat map. The confusion matrix breaks down predictions into four fundamental components: True Positives (TP) mean the model correctly predicts data of the desired class; False Positives (FP) mean the model incorrectly predicts the data of another class as that desired class; true Negatives (TN) means the model correctly predicts the data of other class and False Negatives (FN) means the model incorrectly predicts the data of desired class as other class. The primary performance metrics precision, recall, F1 score, and accuracy are taken to evaluate the model's effectiveness [11].

1. Precision: It shows blockage fault classification to distinguish TP from projected positives. A blockage fault is probable if the model predicts with high precision.

The error may lead to unnecessary inspection and cause time and cost expenses, which is vital.

$$\text{Precision} = \frac{\text{True Positives (TP)}}{\text{True Positives (TP)} + \text{False Positives (FP)}} \quad (3)$$

2. Recall (Sensitivity): It is the ability of a model to recognize all positives(TP). When a FN has catastrophic effects, system breakdowns, and safety issues, recall becomes a priority.

$$\text{Recall} = \frac{\text{True Positives (TP)}}{\text{True Positives (TP)} + \text{False Negative (FN)}} \quad (4)$$

3. F1 Score: It is a harmonic mean of precision and recall that balances them. It accounts for the model's ability to classify blockage faults (precision) correctly and all actual blockage faults (recall). When FP and FN have significant implications, this metric becomes essential.

$$\text{F1 Score} = 2 \times \frac{\text{Precision} \times \text{Recall}}{\text{Precision} + \text{Recall}} \quad (5)$$

4. Accuracy: This parameter measures the proportion of true results (both TP and TN) out of the total number of cases examined. It shows the overall effectiveness of the model.

$$\text{Accuracy} = \frac{\text{True Positives (TP)} + \text{True Negatives (TN)}}{\text{Total Observations}} \quad (6)$$

In evaluating a model's performance, this study focuses on Precision and Recall values alongside accuracy. As the data used in this study is balanced, the importance of the F1 score is slightly diminished.

CHAPTER – 6: Results and discussion

In this study, InceptionV3, a pre-trained CNN model, is retrained to classify blockage faults in the centrifugal pump. Afterward, the architecture of the InceptionV3 model is modified to improve the model's performance. The modified InceptionV3 includes a parallel network with ELU activation functions alongside the traditional ReLU, as shown in Figure 14.

6.1 Classification of blockage faults using InceptionV3 Model

First, the inceptionV3 model is trained on the pump dataset described in section 4 to classify blockage faults in the pump. Out of 16765 samples, 11725 samples are used for training the model, and the remaining dataset is divided equally to validate and test the model. The training and validation performance plots for the Inception V3 model are shown in Figure 18. These plots provide essential insights into the model's learning dynamics over the course of training epochs.

The accuracy plot shown in Figure 18(a) illustrates the progression in the model's ability to classify the training and validation data correctly. A steep increase is seen in training and validation accuracy at the initial level. It indicates that the model is rapidly learning from the data. This steep curve is characteristic of the early stages of training and signifies that the model is assimilating the fundamental patterns in the data. The accuracy plot shows that the trained Inception V3 model finally achieves a training and validation accuracy of 82.24% and 81.71%, respectively.

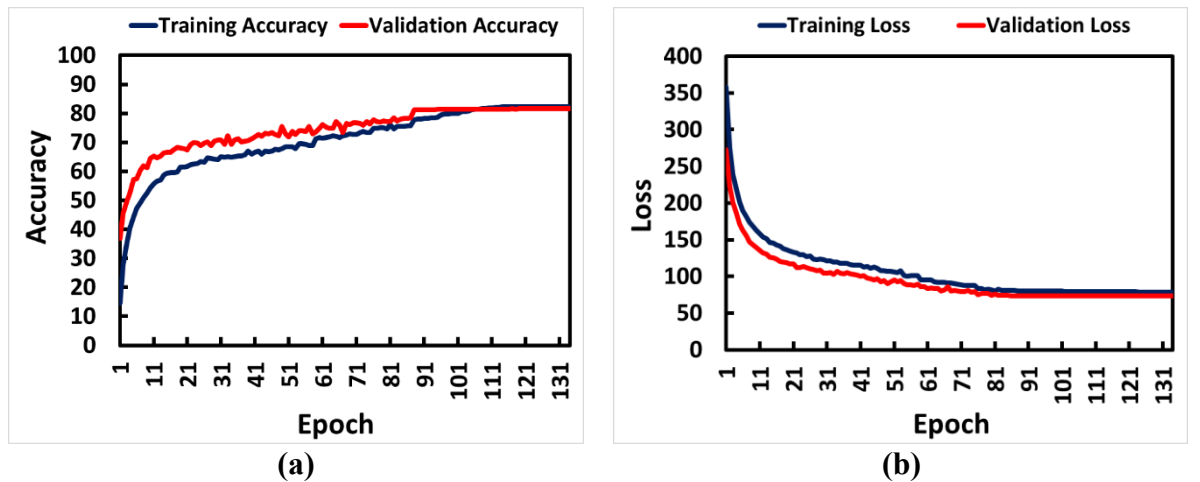


Figure 18: Training and Validation curve for InceptionV3 model showing (a) Accuracy, (b) Loss.

As the epochs progress, the training and validation accuracy curves plateau. It indicates that the model is approaching its asymptotic performance at the current architecture and data. The convergence of

training and validation accuracy suggests that the model is generalizing well and not overfitting the training data.

Additionally, the training loss of the model is shown in Figure 18 (b). This plot exhibits a sharp decline in the initial epochs that gradually flattens. The training loss reflects how well the model fits the training data, with lower values indicating a better fit. The validation loss provides insight into how well the model can generalize its predictions to unseen data. The close convergence of the training and validation loss curves is a reassuring sign that the model performs consistently on both seen and unseen data. However, the slight gap between the training and validation curves in both plots after the initial epochs can indicate some minor overfitting or simply reflect the more complex challenge of generalizing to unseen data. However, since the gap does not widen significantly as training progresses, it does not raise significant concerns regarding the model's generalization capacity.

The overall performance of the Inception V3 model, as shown in Figure 19, provides a summarized view of its efficacy in classifying blockage conditions in a centrifugal pump based on the overall test accuracy, precision, recall, and F1 score. The test accuracy of 81.82% indicates that the model correctly predicts the pump's condition more than 80% of the time during the evaluation of unseen data. This shows a reasonably high level of model generalization since test accuracy is a straightforward reflection of the model's performance on data not utilized during the model's training.

The precision of 81.64% indicates that the model predicts a particular pump's condition correctly about 81.64% of the time. A high precision reflects a lower rate of false positives, which means that the model has a lower likelihood of predicting an incorrect pump's condition in the context of pump maintenance. Thus, a higher value of precision helps in avoiding unnecessary checks or maintenance procedures that would be costly and time-consuming. On the other hand, a recall of 81.80% indicates that the model identifies all relevant instances correctly, 81.80% out of the total pump conditions provided for testing the model. In practical terms, a recall of 81.80% means that the model fails to detect 18.20% of actual pump conditions, which can result in unnecessary maintenance and missed maintenance opportunities, leading to possible pump failures if not addressed promptly.

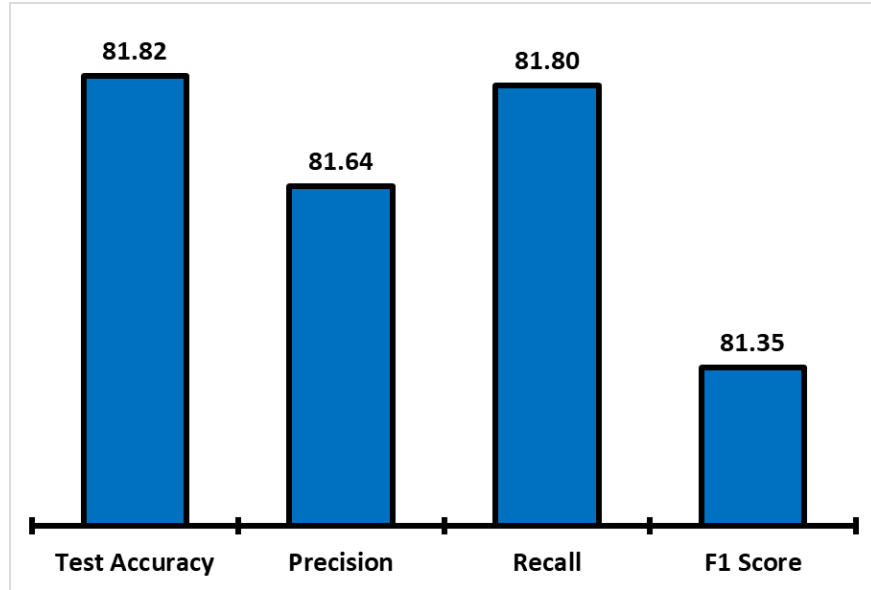


Figure 19: Overall performance parameter of inceptionV3 (values are in percentage).

However, in the context of maintenance strategy, both precision and recall are equally crucial for avoiding unnecessary maintenance and not missing actual pump conditions (especially blockage). The F1 score is a balanced measure that considers both precision and recall. Thus, the F1 score is further employed for evaluating the model in the context of blockage identification in the pump. The InceptionV3 model achieved an F1 score of 81.35%, which is considered good in many applications, suggesting a balanced classification model with no significant bias toward false positives or false negatives [41].

The confusion matrix is shown in Figure 20, shows the classification of the pump's condition into Healthy (AH), DB (Discharge Blockage), SB (Suction Blockage), and SDB (Suction and discharge Blockage). Practical maintenance processes prioritize pump system obstructions by location (suction or discharge line) and severity. The maintenance crew can use the model's predictions to determine the necessary interventions by dividing the 35 classes into these three categories. The model's prediction performance affects maintenance efficiency. For instance, the discharge line is concerned in the case of DB. If the model correctly identifies DB issues, the maintenance staff can quickly fix discharge line faults, preventing more issues. At the same time, a suction line examination is only concerned in the case of SB. Thus, the model's ability to identify SB levels means that maintenance is only done in the suction line when needed, optimizing resource utilization. However, the model's prediction for SDB, the combined blockage scenario, shows a more severe condition requiring

extensive care. Missing a combined blockage can cause system problems; therefore, accurate predictions are crucial. This category helps us evaluate the model's maintenance approach utility by analyzing the confusion matrix. For instance, the model's precision and recall in these areas determine its maintenance alert reliability. High precision in DB and SDB categories reduces false alarms, saving maintenance time. High recall across all categories, notably SDB, means the model can detect true obstructions, decreasing unscheduled downtimes.

Therefore, this complex confusion matrix class division connects the model's output with industry maintenance procedures, making prediction more practical by setting a threshold value for each category (For instance, say SB30 is the threshold value in case of SB that means beyond this severity there is a requirement of examination in suction line). The model will be used for fault detection and predictive maintenance, recommending maintenance personnel to do work and tell them where to work and what time to work based on the severity and location of the blockage. This strategic classification could enhance the efficiency of the centrifugal pumps, reduce maintenance costs, and improve the reliability of operation.

The confusion matrix in Fig. 20 gives the complete description of the model for classification over various conditions of blockages in the centrifugal pump system. For the major class of Discharge Blockage (DB), the model has a high precision of 97%, meaning when a fault of DB is predicted, it is correct 97% of the time. It is an essential factor for maintenance to lower the incidence of false positives, which can be a source of unnecessary inspection or loss. Recall is slightly low at 94.1%, meaning the model may miss around 5.9% of actual DB faults; this can cause a lag in maintenance actions if only the model's recommendations are wholly depended on. In the other case of SB, the precision was very low, equal to 75.28%, giving an increase in false positives as compared to the DB class. The recall of 77.08% indicates that the model is likely to miss SB faults 22.92% of the time. For maintenance planning, it is advised that the model is reliable; additional checks may be warranted, significantly when the model does not predict a DB or SB fault, to avoid missing blockages that could escalate.

2000RPM		PREDICTED VALUES																																					
		AH				DB				SB						SDB																							
		AH	DB15	DB30	DB45	DB60	SB10	SB20	SB30	SB40	SB50	SB60	SDB1510	SDB1520	SDB1530	SDB1540	SDB1550	SDB1560	SDB3010	SDB3020	SDB3030	SDB3040	SDB3050	SDB3060	SDB4510	SDB4520	SDB4530	SDB4540	SDB4550	SDB4560	SDB6010	SDB6020	SDB6030	SDB6040	SDB6050	SDB6060			
AH	DB	TRUE VALUES																																					
SDB	AH	53	0	0	0	0	11	1	0	1	5	0	0	0	0	0	0	0	0	0	0	0	0	0	0	0	0	0	0	0	0	1	0	0	0	0	0	0	
	DB	0	60	3	0	0	0	0	0	0	0	0	0	0	0	0	0	4	0	0	0	0	0	0	0	0	2	2	0	0	0	0	0	0	0	0	1		
	DB30	0	2	67	0	0	0	0	0	0	0	0	0	0	1	0	0	1	1	0	0	0	0	0	0	0	0	0	0	0	0	0	0	0	0	0	0		
	DB45	0	0	0	72	0	0	0	0	0	0	0	0	0	0	0	0	0	0	0	0	0	0	0	0	0	0	0	0	0	0	0	0	0	0	0	0		
	DB60	0	0	0	0	72	0	0	0	0	0	0	0	0	0	0	0	0	0	0	0	0	0	0	0	0	0	0	0	0	0	0	0	0	0	0	0		
	SB	18	0	0	0	0	51	0	0	0	0	0	0	0	0	0	0	0	0	0	0	0	0	0	0	0	0	0	0	0	3	0	0	0	0	0	0		
	SB20	0	0	0	0	0	0	55	0	1	0	0	0	0	0	0	0	0	0	0	2	14	0	0	0	0	0	0	0	0	0	0	0	0	0	0	0	0	
	SB30	0	0	0	0	0	0	0	58	2	0	0	0	0	0	0	0	0	0	9	3	0	0	0	0	0	0	0	0	0	0	0	0	0	0	0	0	0	
	SB40	0	0	0	0	0	0	1	3	54	9	0	0	0	0	0	0	0	0	0	5	0	0	0	0	0	0	0	0	0	0	0	0	0	0	0	0	0	
	SB50	1	0	0	0	0	0	0	0	16	45	4	0	0	0	0	0	0	0	0	5	0	0	0	0	0	0	0	0	0	1	0	0	0	0	0	0	0	
	SB60	0	0	0	0	0	0	0	0	0	0	70	0	0	0	0	0	0	0	0	0	0	2	0	0	0	0	0	0	0	0	0	0	0	0	0	0	0	
	SDB1510	0	1	1	0	0	0	0	0	0	0	0	63	4	0	0	0	0	2	1	0	0	0	0	0	0	0	0	0	0	0	0	0	0	0	0	0	0	
	SDB1520	0	0	0	0	0	0	0	0	0	0	0	0	71	0	0	0	0	0	1	0	0	0	0	0	0	0	0	0	0	0	0	0	0	0	0	0	0	
	SDB1530	0	0	0	0	0	0	0	0	0	0	0	0	1	71	0	0	0	0	0	0	0	0	0	0	0	0	0	0	0	0	0	0	0	0	0	0	0	
	SDB1540	0	0	0	0	0	0	0	0	0	0	0	0	1	4	61	6	0	0	0	0	0	0	0	0	0	0	0	0	0	0	0	0	0	0	0	0	0	
	SDB1550	0	0	0	0	0	0	0	1	0	0	0	0	0	0	4	67	0	0	0	0	0	0	0	0	0	0	0	0	0	0	0	0	0	0	0	0	0	
	SDB1560	0	0	0	0	0	0	0	0	0	0	0	0	0	0	0	0	72	0	0	0	0	0	0	0	0	0	0	0	0	0	0	0	0	0	0	0	0	
	SDB3010	0	0	0	0	0	0	0	0	0	0	0	6	0	0	0	0	0	65	0	0	0	0	0	0	0	1	0	0	0	0	0	0	0	0	0	0	0	
	SDB3020	0	0	1	0	0	0	2	0	0	0	0	1	0	0	1	0	0	32	10	0	0	0	0	0	1	2	9	10	2	0	0	0	0	0	0	0	0	
	SDB3030	0	0	0	0	0	0	0	8	0	0	0	0	0	0	0	0	9	52	2	0	0	0	0	0	0	0	0	0	1	0	0	0	0	0	0	0	0	
SDB3040	0	0	0	0	0	0	0	9	12	6	1	0	0	0	0	0	0	3	2	30	1	0	0	0	0	0	0	0	3	5	0	0	0	0	0	0	0		
SDB3050	0	0	0	0	0	1	2	0	0	10	2	0	0	0	0	0	0	1	3	46	1	0	0	0	0	0	0	6	0	0	0	0	0	0	0	0	0		
SDB3060	0	0	0	0	0	0	0	0	0	0	0	0	0	0	0	1	0	0	0	0	0	71	0	0	0	0	0	0	0	0	0	0	0	0	0	0	0	0	
SDB4510	0	0	0	0	0	0	2	0	0	0	0	0	0	0	0	0	0	0	0	0	0	0	64	6	0	0	0	0	0	0	0	0	0	0	0	0	0	0	
SDB4520	0	0	0	0	0	0	0	0	0	0	0	0	0	0	0	0	0	0	0	0	0	0	10	62	0	0	0	0	0	0	0	0	0	0	0	0	0	0	0
SDB4530	0	0	0	0	0	0	0	0	0	0	0	0	0	0	0	1	0	0	0	0	0	0	7	64	0	0	0	0	0	0	0	0	0	0	0	0	0	0	0
SDB4540	0	0	0	0	0	0	0	0	0	0	0	0	0	0	0	0	0	0	0	0	0	0	0	0	68	4	0	0	0	0	0	0	0	0	0	0	0	0	0
SDB4550	0	0	0	0	0	0	0	0	0	0	0	0	0	0	0	0	2	0	0	0	0	0	0	0	0	0	0	1	69	0	0	0	0	0	0	0	0	0	
SDB4560	0	0	0	0	0	0	0	0	3	2	0	0	0	0	1	0	0	1	1	3	1	0	0	0	0	0	0	1	59	0	0	0	0	0	0	0	0	0	
SDB6010	0	0	0	0	0	0	0	0	0	0	0	0	0	0	0	0	0	0	0	0	0	0	0	0	0	0	0	0	0	39	15	3	12	3	0	0	0		
SDB6020	0	0	0	0	0	0	0	0	0	0	0	0	0	0	0	0	0	0	0	0	0	0	0	0	0	0	0	0	0	13	58	0	1	0	0	0	0		
SDB6030	0	0	0	0	0	0	0	0	0	0	0	0	0	0	0	0	0	0	0	0	0	0	0	0	0	0	0	0	0	0	0	52	5	15	0	0	0		
SDB6040	0	0	0	0	0	0	0	0	0	0	0	0	0	0	0	0	0	0	0	0	0	0	0	0	0	0	0	0	0	13	3	2	30	10	14	0	0		
SDB6050	0	0	0	0	0	0	0	0	0	0	0	0	0	0	0	0	0	0	0	0	0	0	0	0	0	0	0	0	0	0	0	1	5	66	0	0	0		
SDB6060	0	0	0	0	0	0	0	0	0	0	0	0	0	0	0	0	0	0	0	0	0	0	0	0	0	0	0	0	0	0	0	0	0	0	0	72	0	0	

Figure 20: Confusion matrix for test data classified by InceptionV3 model.

The combined suspension and discharge blockage (SDB) shows strong performance, with the highest number of true positives and high precision and recall scores of 81% and 81.28%, respectively. This indicates that the model is particularly adept at identifying conditions when both blockages are present. This is critical because such scenarios likely represent more severe faults that require immediate attention. From a maintenance perspective, these metrics suggest that the ML model effectively prioritizes inspections and repairs. High precision across all categories means that maintenance efforts can be efficiently allocated with minimal wasted resources on false positives. However, the model's recall indicates that some blockages might need to be noticed, especially in the SB and DB categories. For robust maintenance strategies, the model's predictions should be supplemented with regular checks to catch the faults that the model may miss. This pattern of misclassification amongst certain classes suggests that the features learned by the model are not entirely distinct for each fault type, possibly due to overlapping characteristics in the fault signatures or the limitations inherent in the ReLU activation function's treatment of

negative input values that reflect a generally effective model and indicate room for improvement, particularly in terms of model sensitivity, precision and so F1 - Scores. Thus, it aimed to propose a better model that can capture blockage faults' complex and subtle patterns, ultimately refining the model's predictive accuracy and reliability.

6.2 Classification of blockage faults using Modified InceptionV3 Model

In this section, InceptionV3 is modified to improve its performance for more effective identification of blockages in the pump. The accuracy plot of the modified InceptionV3 model is shown in Figure 21 (a). It illustrates that the trained model achieves a training accuracy of 99.68% and an even higher validation accuracy of 95.48%.

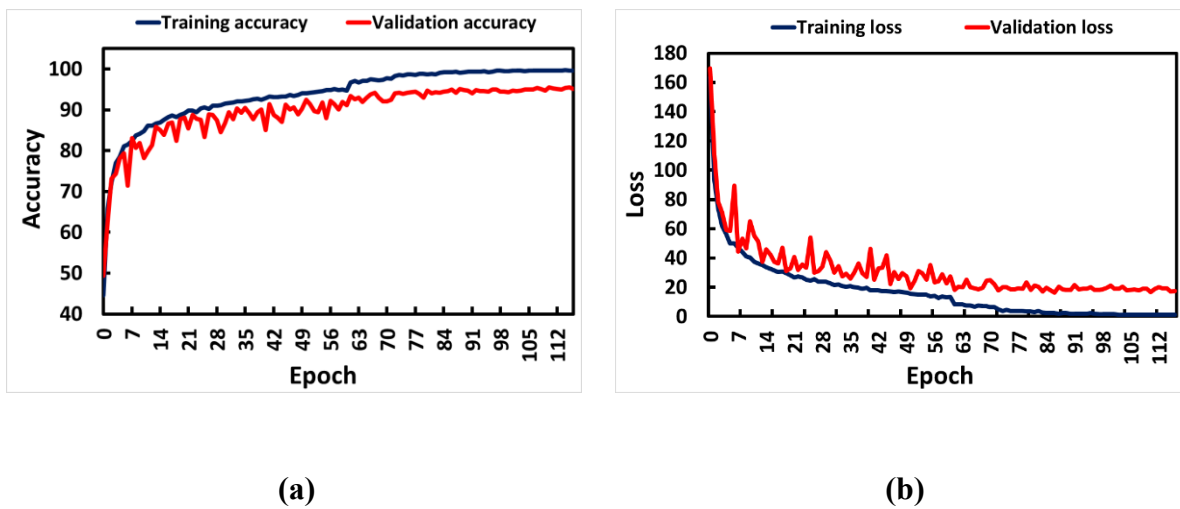


Figure 21: Training and Validation curve for Modified InceptionV3 model showing (a) Accuracy, (b) Loss.

It shows that modified InceptionV3 achieves exceptional proficiency in classifying blockage faults within a centrifugal pump system compared to only the Inception V3 model (as shown in Fig. 18). The performance metrics of the modified InceptionV3 model, as shown in Fig. 21, reflect an effective and well-tuned neural network architecture. Notably, the validation accuracy surpasses the training accuracy, which is an encouraging indicator of the model's generalization capability. It is to be noted that the modifications to the network, including the introduction of ELU activation functions and the strategic use of dropout, enhance the model's predictive performance on unseen data rather than simply memorizing the training dataset. As shown in Fig.21 (b), the loss values further reinforce the model's solid performance, with a training loss of 1.08% and a lower validation loss of 16.27%. The lower validation loss relative to the training loss is somewhat unconventional, while one would expect the loss to be lower in the case that the model is given the training data directly. At times, this perhaps signified that the validation set was, by chance, a bit easier

to predict for the model, or it could be that the model was benefiting from the regularization effects introduced by the modifications, hence not overfitting, and therefore performing even better on validation data. The model shows good performance, which would be indicative of a model with robust and good architecture that has good generalization potential in fault classification. High validation accuracy and low lost accuracy open quite promising practical assurance to the potential application of this model in the elucidative types of predictive maintenance, and this can result from the application into excellent enhancements in maintenance strategies, optimization of operations, and reduction of downtimes in centrifugal pump systems.

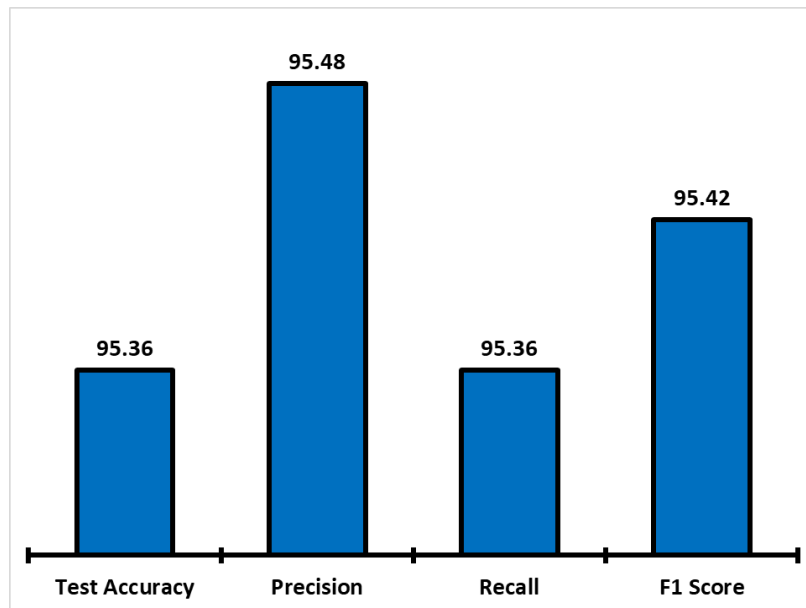


Figure 22: Overall performance parameter of inceptionV3 (values are in percentage).

The developed modified Inception V3 model was demonstrated for the complete evaluation of classification capabilities based on the test accuracy, precision, recall, and F1 score. The test accuracy is 95.36%, which underlines the correctness in the model predictions were tested on unseen test data. This finding is crucial, in the sense that it helps to affirm that the model is generalizable, beyond the data it was trained on, which is indicative of practical robustness, and therefore reliable. The test accuracy, precision, recall, and F1 for the modified InceptionV3 model are 95.48%, 95.36%, and 95.42%, respectively. The high-test accuracy, as well as the high F1 score, establishes that the model is very effective in performing the fault classification task. This surely strengthens the fact that the likely changes in model architecture were affected through creating many parallel layers and changing the dropout rates, yielding escalated sensitivity to correctly classify blockage faults without high bias towards over- or under-prediction of cases, thereby proving application of the model in the direction of maintenance decision-making in

industry, inasmuch as it is effective fault detection that brings about operational effectiveness, and most importantly, safety.

2000RPM			PREDICTED VALUES																																				
			AH	DB				SB						SDB																									
			AH	DB15	DB30	DB45	DB60	SB10	SB20	SB30	SB40	SB50	SB60	SDB1510	SDB1520	SDB1530	SDB1540	SDB1550	SDB1560	SDB3010	SDB3020	SDB3030	SDB3040	SDB3050	SDB3060	SDB4510	SDB4520	SDB4530	SDB4540	SDB4550	SDB4560	SDB6010	SDB6020	SDB6030	SDB6040	SDB6050	SDB6060		
TRUE VALUES	AH	59	0	0	0	0	13	0	0	0	0	0	0	0	0	0	0	0	0	0	0	0	0	0	0	0	0	0	0	0	0	0	0	0	0	0	0		
	DB	DB15	0	71	1	0	0	0	0	0	0	0	0	0	0	0	0	0	0	0	0	0	0	0	0	0	0	0	0	0	0	0	0	0	0	0	0		
	DB30	0	0	72	0	0	0	0	0	0	0	0	0	0	0	0	0	0	0	0	0	0	0	0	0	0	0	0	0	0	0	0	0	0	0	0	0		
	DB45	0	0	0	72	0	0	0	0	0	0	0	0	0	0	0	0	0	0	0	0	0	0	0	0	0	0	0	0	0	0	0	0	0	0	0	0		
	DB60	0	0	0	0	72	0	0	0	0	0	0	0	0	0	0	0	0	0	0	0	0	0	0	0	0	0	0	0	0	0	0	0	0	0	0	0		
	SB	SB10	1	0	0	0	0	71	0	0	0	0	0	0	0	0	0	0	0	0	0	0	0	0	0	0	0	0	0	0	0	0	0	0	0	0	0	0	
	SB20	0	0	0	0	0	0	72	0	0	0	0	0	0	0	0	0	0	0	0	0	0	0	0	0	0	0	0	0	0	0	0	0	0	0	0	0		
	SB30	0	0	0	0	0	0	0	62	1	0	0	0	0	0	0	0	0	0	6	3	0	0	0	0	0	0	0	0	0	0	0	0	0	0	0	0		
	SB40	0	0	0	0	0	0	0	0	1	60	1	0	0	0	0	0	0	0	9	1	0	0	0	0	0	0	0	0	0	0	0	0	0	0	0	0	0	
	SB50	0	0	0	0	0	0	0	0	0	1	64	0	0	0	0	0	0	0	0	7	0	0	0	0	0	0	0	0	0	0	0	0	0	0	0	0	0	
	SB60	0	0	0	0	0	0	0	0	0	0	0	72	0	0	0	0	0	0	0	0	0	0	0	0	0	0	0	0	0	0	0	0	0	0	0	0	0	
	SDB	SDB1510	0	0	0	0	0	0	0	0	0	0	71	1	0	0	0	0	0	0	0	0	0	0	0	0	0	0	0	0	0	0	0	0	0	0	0	0	
	SDB1520	0	0	0	0	0	0	0	0	0	0	0	0	72	0	0	0	0	0	0	0	0	0	0	0	0	0	0	0	0	0	0	0	0	0	0	0	0	
	SDB1530	0	0	0	0	0	0	0	0	0	0	0	0	0	72	0	0	0	0	0	0	0	0	0	0	0	0	0	0	0	0	0	0	0	0	0	0	0	
	SDB1540	0	0	0	0	0	0	0	0	0	0	0	0	0	0	72	0	0	0	0	0	0	0	0	0	0	0	0	0	0	0	0	0	0	0	0	0	0	
	SDB1550	0	0	0	0	0	0	0	0	0	0	0	0	0	0	0	72	0	0	0	0	0	0	0	0	0	0	0	0	0	0	0	0	0	0	0	0	0	
	SDB1560	0	0	0	0	0	0	0	0	0	0	0	0	0	0	0	0	72	0	0	0	0	0	0	0	0	0	0	0	0	0	0	0	0	0	0	0	0	
	SDB3010	0	0	0	0	0	0	0	0	0	0	0	0	0	0	0	0	0	72	0	0	0	0	0	0	0	0	0	0	0	0	0	0	0	0	0	0	0	
	SDB3020	0	0	0	0	0	0	0	0	0	0	0	0	0	0	0	0	0	0	60	0	0	1	0	1	0	1	2	7	0	0	0	0	0	0	0	0	0	
	SDB3030	0	0	0	0	0	0	0	4	0	0	0	0	0	0	0	0	0	0	1	67	0	0	0	0	0	0	0	0	0	0	0	0	0	0	0	0	0	
	SDB3040	0	0	0	0	0	0	0	4	4	1	0	0	0	0	0	0	0	0	0	1	62	0	0	0	0	0	0	0	0	0	0	0	0	0	0	0	0	0
	SDB3050	0	0	0	0	0	0	2	0	0	0	0	0	0	0	0	0	0	0	0	0	70	0	0	0	0	0	0	0	0	0	0	0	0	0	0	0	0	0
	SDB3060	0	0	0	0	0	0	0	0	0	0	0	0	0	0	0	0	0	0	0	0	72	0	0	0	0	0	0	0	0	0	0	0	0	0	0	0	0	0
	SDB4510	0	0	0	0	0	0	0	0	0	0	0	0	0	0	0	0	0	0	0	0	0	71	1	0	0	0	0	0	0	0	0	0	0	0	0	0	0	0
	SDB4520	0	0	0	0	0	0	0	0	0	0	0	0	0	0	0	0	0	0	0	0	0	7	65	0	0	0	0	0	0	0	0	0	0	0	0	0	0	0
	SDB4530	0	0	0	0	0	0	0	0	0	0	0	0	0	0	0	0	0	0	0	0	0	1	71	0	0	0	0	0	0	0	0	0	0	0	0	0	0	0
	SDB4540	0	0	0	0	0	0	0	0	0	0	0	0	0	0	0	0	0	0	0	0	0	0	0	72	0	0	0	0	0	0	0	0	0	0	0	0	0	0
	SDB4550	0	0	0	0	0	0	0	0	0	0	0	0	0	0	0	0	0	0	0	0	0	0	0	0	72	0	0	0	0	0	0	0	0	0	0	0	0	0
SDB4560	0	0	0	0	0	0	0	0	0	0	0	0	0	0	0	0	0	0	0	0	0	0	0	0	0	0	72	0	0	0	0	0	0	0	0	0	0		
SDB6010	0	0	0	0	0	0	0	0	0	0	0	0	0	0	0	0	0	0	0	0	0	0	0	0	0	0	0	0	58	5	0	9	0	0	0	0	0		
SDB6020	0	0	0	0	0	0	0	0	0	0	0	0	0	0	0	0	0	0	0	0	0	0	0	0	0	0	0	0	3	69	0	0	0	0	0	0	0		
SDB6030	0	0	0	0	0	0	0	0	0	0	0	0	0	0	0	0	0	0	0	0	0	0	0	0	0	0	0	0	0	0	72	0	0	0	0	0	0		
SDB6040	0	0	0	0	0	0	0	0	0	0	0	0	0	0	0	0	0	0	0	0	0	0	0	0	0	0	0	0	0	4	0	1	60	1	6	0	0		
SDB6050	0	0	0	0	0	0	0	0	0	0	0	0	0	0	0	0	0	0	0	0	0	0	0	0	0	0	0	0	0	0	0	2	2	68	0	0	0		
SDB6060	0	0	0	0	0	0	0	0	0	0	0	0	0	0	0	0	0	0	0	0	0	0	0	0	0	0	0	0	0	0	0	0	0	0	0	72	0	0	

Figure 23: Confusion matrix for test data classified by Modified InceptionV3 model.

The confusion matrix of the tuned InceptionV3 gives a high general view of its performance over the three principal, differently faulted pump conditions in a centrifugal pump, namely: DB (Discharge Blockage), SB (Suction Blockage), and SDB (Suction and Discharge Blockage), as highlighted in Figure 23. The precision and maximum recall obtained for DB are 99.66% and 99.65% respectively, with one false positive, and one false negative. That is a good model performance in the sense whereby every discharge blockage condition was detected. Such accuracy suggests that the features associated with a DB are distinctive and are well learned by the model, which is an essential head start for maintenance teams to take precise actions on the discharge line without diverting resources to unnecessary surveys on the affected area. With the SB class, there is only a slight drop in precision to 92.84%,

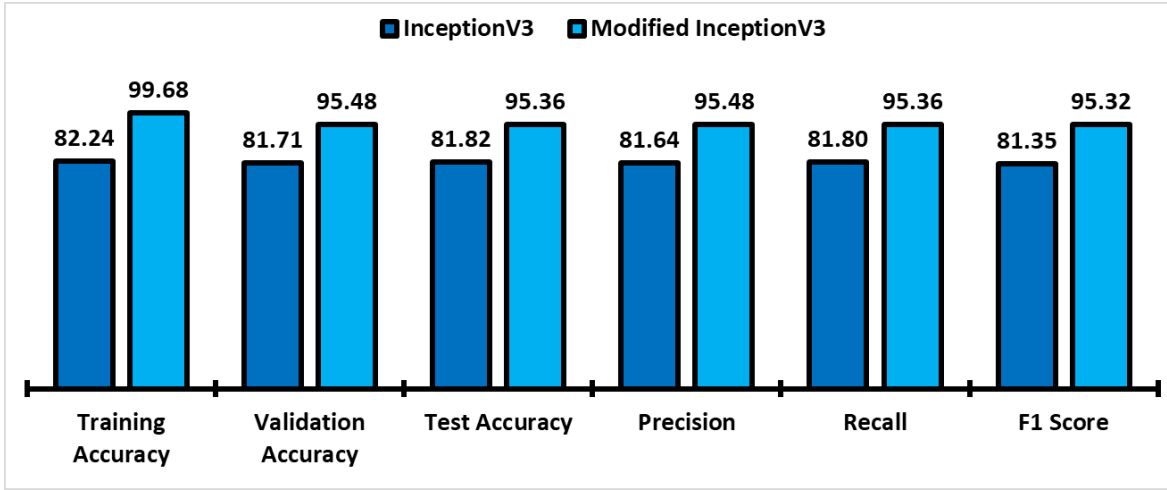
which means that the model predicts suction blockage when SB does not exist in the indicated condition (32 false positives). The high value of recall (92.82%) also shows that the model can detect the majority of real suction blockages (401 true positives) with a few cases being missed (31 false negatives).

The model is very reliable in this category; the presence of false positives suggests that there might be some patterns that the model misinterprets as suction blockages, potentially leading to unnecessary maintenance work. For the combined SDB conditions, the model again performs exceptionally well, with a precision of 95.32% and a recall of 95.83%. This means that not only does the model correctly identify nearly all instances of combined suction and discharge blockages (1656 true positives), but it also maintains a meager rate of false alarms (83 false positives) and misses (72 false negatives).

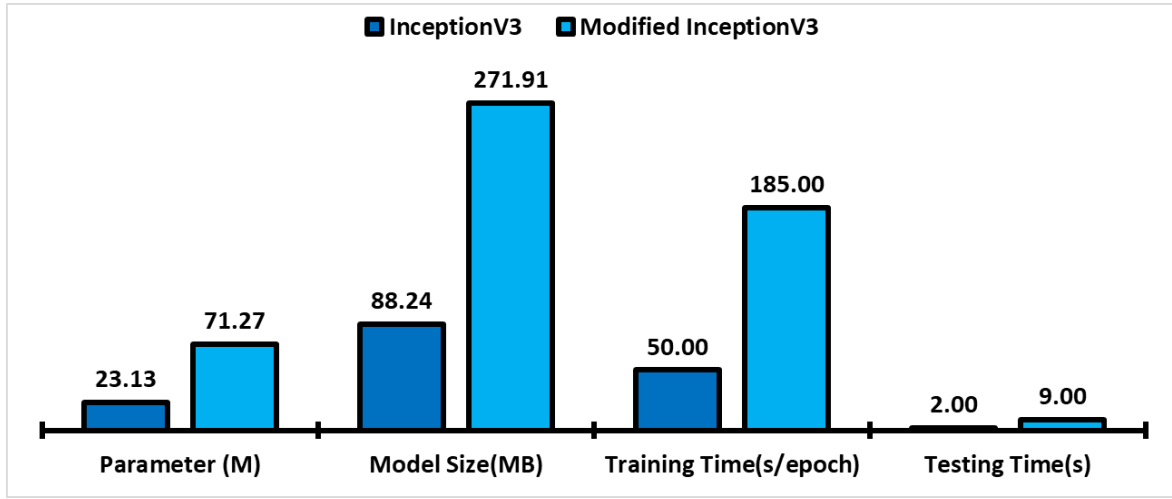
Such performance is critical as it implies the model is highly adept at identifying severe blockages that affect both lines, which are typically more urgent and might require immediate attention. Overall, the modified Inception V3 model performs accurately in identifying various blockage conditions, making it a potent tool for predictive maintenance. Its ability to discern with such precision and recall makes it a strong candidate for deployment in a real-world industrial setting, where predictive maintenance can result in significant cost savings and operational efficiency.

6.3 Comparison

This section compares the modified InceptionV3 with the conventional InceptionV3 in various aspects. Figure 24 illustrates the comparison between these two models in various aspects. It signifies that the architectural adjustments improve the performance of the InceptionV3 despite higher processing costs. The Modified InceptionV3 model outperforms the original in training, validation, and test accuracy, as shown in Fig 24 (a). With training accuracy rising from 82.02% to 90.75% and validation accuracy rising from 81.43% to 94.05%, the updated model learns better and generalizes to new datasets. Test accuracy, crucial for assessing model performance in real-world scenarios, increases from 81.43% to 92.06%. The updated model has more balanced and accurate classification capabilities, as shown by an F1-score of 92.11%, up from 81.51%. High precision and recall can distinguish between efficient maintenance and costly downtime in industrial settings. Operationally, the modified Inception V3 model needs greater processing power.



(a)



(b)

Figure 24: Comparison of performance of IncetionV3 and Modified InceptionV3 model based on (a) Performance parameter and (b) Size and time.

Model size, training time, and testing time grow as parameters nearly treble, as depicted in Figure 24 (b). These expenditures are evaluated against the model's improved accuracy. Predictive maintenance can save machine failure costs that greatly outweigh computational costs by predicting and preventing defects. Once the model is deployed, the testing time of 9 seconds, which is higher for the Modified model but can still be workable for many industrial applications, becomes the crucial factor, not the model size or training time. Therefore, the modified InceptionV3 model strongly argues for its use in predictive maintenance environments. The model's improved performance metrics indicate that it can recognize complicated failure patterns and boost operational efficiency.

The F1-Score for each class is compared for both the modified and conventional InceptionV3 models in Figure 25. The F1-Score, as a singular measure of a model's accuracy, also gives insight into the precision-recall trade-off and is particularly informative when high accuracy is paramount in both dimensions.

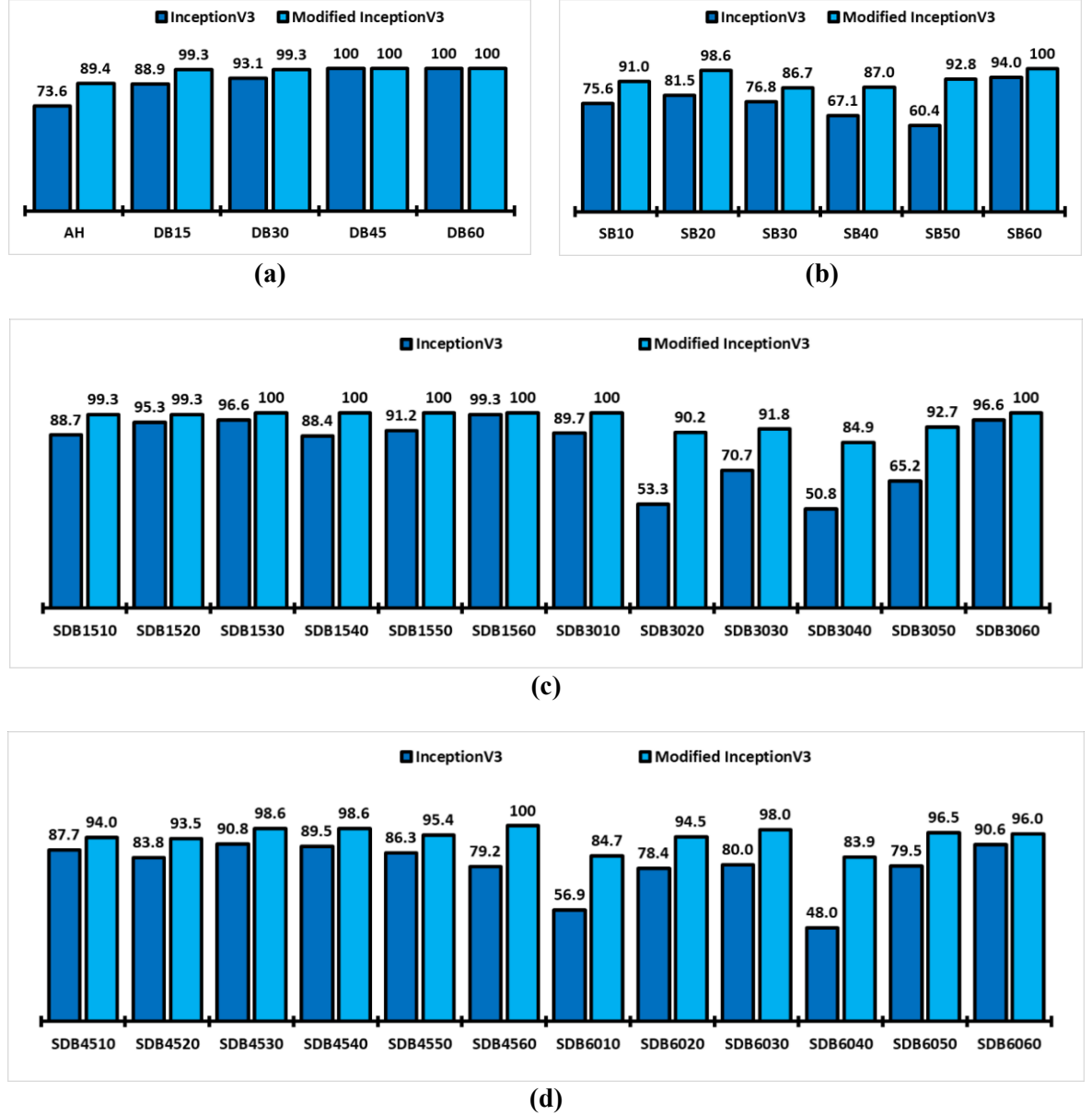


Figure 25: Comparison of F1 - Score of InceptionV3 and Modified InceptionV3 model in case of (a) DB, (b) SB, (c) SDB1510 to SDB3060, (d) SDB4510 to SDB6060.

In class AH (At Healthy), the modified InceptionV3 model demonstrates an F1-Score of 89.4% against the original model's 73.6%, showcasing the architectural enhancements' effectiveness in achieving a balance between precision and recall. This trend of F1-Score improvement with the modified model is consistently observed across the board. For classes with intricate fault patterns, such as SB40 and SB50, the improvements are significant, where the modified

InceptionV3 model exhibits F1-Scores of 87% and 92.8%, respectively, as opposed to the original model's F1-Scores of 67.1% and 60.4% in the same classes. This indicates a substantial enhancement in the model's ability to classify these challenging conditions accurately. It is noteworthy that in classes where the original InceptionV3 model had already achieved a high F1-Score. For instance, the modified model retains this high level of performance in DB45 and DB60, as shown in percentages for both models of F1-Score is 100%. The high scores are maintained in the modified model while improving the low-scoring classes, which are a positive indicator of the success of the introduced changes.

The modified model shows significant progress in classes such as SDB1540, SDB3020, and SDB6040, where F1-Score is increasing from 88.4% to 100%, from 53.3% to 90.2%, and from 48% to 83.9%, respectively. The inset graph ranks a model's capacity to select the balanced data representation, such that both the positive cases are detected, and the false positives are minimized. The performance of the modified InceptionV3 model is observed to be excellent and well-balanced in classifying all selected pump conditions under the investigation given the F1-Score graph. Consequently, the developed structure of the model, including ELU activation functions, turns it into a much more accurate and reliable fault detection system. This is a very important performance measure, a mix of precision and recall, in the context of centrifugal pump maintenance, where the cost of misclassification is high.

It is typically an unavoidable trade-off in most stringent practical applications between the computational resource and increased predictive accuracy. The capability and robustness of the modified InceptionV3 model will ensure that no subtle pattern within the data goes unnoticed. This approach is particularly advantageous in industrial settings such as oil refineries, nuclear plants, chemical industries, etc., as the cost of misclassification can be substantial. The investment in additional computational resources is offset by the improvement in performance, leading to a more reliable and effective monitoring system for predictive maintenance.

Table 5: Performance comparison of modified inceptionV3 with other pre-trained models at 2000RPM, 1750RPM and 1500RPM.

2000RPM				
Performance parameters	VGG16	InceptionV3	InceptionResNet	Modified InceptionV3
Training accuracy	53.16	82.24	78.06	99.68
Validation accuracy	62.54	81.71	81.67	95.48
Test accuracy	62.94	81.82	78.10	95.36
Precision	65.00	81.64	79.00	95.48
Recall	64.00	81.80	79.00	95.36
F-1 Score	64.50	81.35	79.00	95.32

1750RPM				
Performance parameters	VGG16	InceptionV3	InceptionResNet	Modified InceptionV3
Training accuracy	48.62	72.64	69.37	96.25
Validation accuracy	51.32	76.03	72.22	93.71
Test accuracy	49.57	74.44	71.15	93.06
Precision	50.00	75.00	70.00	93.22
Recall	49.00	74.00	71.00	93.06
F-1 Score	49.48	73.00	69.00	93.07

1500RPM				
Performance parameters	VGG16	InceptionV3	InceptionResNet	Modified InceptionV3
Training accuracy	43.68	65.06	64.53	95.41
Validation accuracy	46.71	68.13	67.19	92.14
Test accuracy	44.83	67.02	66.35	92.50
Precision	45.00	70.00	66.00	93.09
Recall	45.00	67.00	66.00	92.50
F-1 Score	45.00	66.00	66.00	92.60

To validate the performance of the modified InceptionV3 model, its performance metrics with those of popular pre-trained models are compared, as shown in Table 5. The modified InceptionV3 outperforms the other models across all metrics. Also, combination of activation functions are meticulously studies and find out the best performance of the model was coming with ReLU and ELU as shown in Table 6.

Our present study, which utilizes a pressure signal and convolutional features, achieved a classification accuracy of 92.06% on

35 classes of fault at approximately 35Hz, demonstrating superior performance compared to other methods. This comprehensive evaluation underscores the robustness and effectiveness of the modified InceptionV3 model in handling diverse fault conditions.

Table 6: Performance comparison of modified inceptionV3 with the combination of ReLU with other Activation Functions at 2000RPM

S.N.	Activation function1	Activation function2	Validation accuracy
1	ReLU	tanh	91.93
2	ReLU	swish	88.89
3	ReLU	ReLU	93.39
4	ReLU	ELU	95.48
5	ReLU	Leaky ReLU	93.15
6	ReLU	selu	91.73
7	ReLU	sigmoid	90.40

In the experiment of fault diagnosis, a five-fold cross-validation method is used to generalize and enhance the robustness of the model assessment on different fault conditions (35 fault conditions) at three speeds (2000rpm, 1750rpm, and 1500rpm). At the same time, as clearly visible in Table 8, the validation accuracies achieved, on average, reached 92.76%, 90.92%, and 90.50%, respectively. On the total of 16,765 image datasets, 3353 datasets (20% of the total dataset) is used as validation, and 13412 dataset (80% of the total dataset) used as Training dataset at each fold. For robust performance, hyperparameter optimization was conducted using keras Hyperband tuner on two dropout layers and one final dense layer as shown in Table 7. The average optimal values returned by the Hyperband tuner were around 570 dense units and 0.34 for both dropout layers. Nonetheless, in terms of hardware limitations, the number of dense units were set to 512 and the dropout rate was preserved at 0.34 in order to achieve a similar accuracy but with a more feasible implementation.

Table 7: Results of hyper-parameter optimization for five-fold cross validation

Fold	Dense Units	Dropout 1	Dropout 2
Fold-1	50	0.5	0.3
Fold-2	850	0.3	0.1
Fold-3	950	0.1	0.1
Fold-4	550	0.1	0.7
Fold-5	450	0.7	0.5
Average	570	0.34	0.34

Table 8: Results of five-fold cross-validation

Folds	2000RPM	1750RPM	1500RPM
Fold-1	92.69	90.46	90.32
Fold-2	92.17	91.51	90.21
Fold-3	93.08	90.63	90.84
Fold-4	92.87	90.53	90.37
Fold-5	93.00	91.45	90.74
Average	92.76	90.92	90.50

Additionally, we conducted a comparative study with existing literature, as summarized in Table 8. This comparison is based on various factors, including the number of blockage faults per rpm, the type of signal used, the features chosen, the classification methods employed, and the classification accuracy reported in each study. The present work outperforms previous works by examining 35 blockage faults per RPM using pressure signals, compared to fewer faults in other studies as shown in Table 6. For instance, Tiwari et al. (2020) and Panda et al. (2018) focused on five faults with lower accuracies (91.7% and 82.9%). Bordoloi et al. (2017) and Rajur et al. (2018) also showed limited performance with SVM. Ranawat et al. (2023) achieved high accuracy at high RPM but examined fewer faults. The present study's use of convolutional features and a modified InceptionV3 network achieves superior accuracy of 92.06% at ~35Hz, demonstrating robust and comprehensive performance.

Table 9: Comparative study of current work with other literature.

S.N.	Authors	Blockage Faults per rpm	Signal/domain	Fault Features	Classification Method	Overall Performance
1.	Tiwari et al. (2020)[9]	5	Dynamic Pressure/time domain	SD, mean, kurtosis, and skewness	Deep Learning	Below 50Hz the accuracy is 91.7%.
2.	Panda et al. (2018)[6]	5	Vibration/time domain	SD, mean, kurtosis, skewness, crest factor and entropy	SVM	Below 50Hz accuracy is 82.9%.
3.	Bordoloi et al. (2017)[42]	5	Vibration/time domain	SD, kurtosis, and skewness	SVM	Below 50Hz accuracy is 79.33% .
4.	Rapur et al. (2018)[43]	10	Vibration/time domain	SD, mean, and entropy	SVM	Below 35Hz accuracy is 91.2%
5.	Ranawat et al. (2023)[17]	4	Pressure Signal	Features extracted from pre-trained models	Shallow classifiers	Accuracy is 97% at 2000 RPM
6.	Ranawat et al. (2023)[11]	3	Pressure Signal	12 Statistical features, Holder exponent	LSTM and Bi-LSTM based classifier	Accuracy is 99.01% at 2000 RPM
7.	Present Study	35	Pressure Signal	Convolutional features	Modified InceptionV3 Network	Accuracy is 92.06% at ~35Hz

CHAPTER – 7: Conclusion and future work

7.1 Conclusion

The present study incorporates the modification of the InceptionV3 model with the aim of increasing the capacity of blockage identification in the centrifugal pump. The following are the findings which can be drawn from the present study:

- i. The present study focused on suction pressure as a critical parameter for blockage fault detection. This is an innovative conceptualization in the present study. The approach provides deeper insight into the operation state of the pump, which further helps the fault detection capacity of the model to manifold.
- ii. Suction pressure signal, which can be converted into 2D image through CWT. The plots reveal the influence of the blockages upon the different frequency components of the pump system.
- iii. Integration of continuous wavelet transform with the InceptionV3 model has advanced the blockage identification in the pump. This can further lead to more critical thinking related to pump suction pressure data, which has resulted in huge accuracy in fault detection even at a low value of image pixel.
- iv. This work further appends Exponential Linear Units (ELUs) into the existing structure of Rectified Linear Units (ReLUs) of the InceptionV3 model to enhance performance in blockage diagnosis. Because of this novel approaches the test accuracy has been substantially increased from 81.43% to 92.06%, which on 35 classes has shown greater effectiveness regarding the ability of the model to generalize significantly new data sets.

This research demonstrates the Modified InceptionV3 model's effectiveness in a novel application that also paves the way for future advancements in innovative maintenance strategies within industrial machinery. The combination of technical innovation and practical applicability underscores this study's significant impact and potential.

However, the present study highlights several advancements and contributions to blockage fault diagnosis in centrifugal pumps, certain limitations underline the scope for future improvements.

7.2 Limitations

1. Blockages were emulated using butterfly-valve constrictions, which do not capture the complex multiphase dynamics of air entrainment (bubble formation, collapse, and phase

- interactions). As a result, the model may not generalize to gas-entrained faults without additional training data.
2. By design, our framework uses only suction-pressure signals. While this proved effective for blockage classification, it may miss other fault signatures—such as vibration anomalies, discharge-pressure fluctuations, or temperature changes—that could further enhance early detection of mechanical or hydraulic issues.
 3. Generating CWT scalograms and running the deep CNN on a standard GPU requires substantial processing time and memory, limiting straightforward real-time deployment in resource-constrained settings.
 4. All experiments were conducted on a single centrifugal-pump test rig. Differences in pump geometry, impeller design, and operating conditions across industrial installations may affect the model's predictive accuracy.

7.3 Future Work

In future, this model can be further modified and improved in several ways:

- i. **Evaluating Different Combinations of Activation Functions:** The performance of the model can be enhanced by experimenting with various activation functions. The use of different combinations, such as ReLU, Leaky ReLU, ELU, tanh, selu, and others, may yield better accuracy and robustness.
- ii. **Testing at Different Speeds:** The current model has been evaluated at a specific speed. Future studies can include testing the model at various pump speeds to understand its performance under different operational conditions. This will help in making the model more adaptable and reliable for real-world applications.
- iii. **Exploring Different Plots for CNN Input:** While the current model uses 2D Continuous Wavelet Transform (CWT) plots of pressure signals, other types of plots could be explored. For example, Short-Time Fourier Transform (STFT) or spectrogram plots might provide different insights and potentially improve the classification accuracy.
- iv. **Integrating Additional Sensor Data:** Incorporating data from additional sensors, such as vibration or temperature sensors, could provide a more comprehensive understanding of the pump's condition and further enhance the model's diagnostic capabilities.

- v. **Real-Time Implementation and Testing:** Implementing the model in a real-time monitoring system and testing its performance in an operational industrial environment would be a crucial step. This will help in validating the model's effectiveness and reliability in practical scenarios.
- vi. **Automated Hyperparameter Tuning:** Utilizing automated machine learning (AutoML) techniques to optimize the hyperparameters of the CNN model can save time and potentially improve the model's performance.
- vii. **Expanding the Fault Classes:** Including a broader range of fault types and severity levels in the dataset can make the model more versatile and capable of diagnosing a wider variety of issues in centrifugal pumps.
- viii. **Multiphase Fault Modeling:** We will extend our dataset and retrain the modified InceptionV3 network on air-contamination scenarios by incorporating high-speed pressure sensors and/or CFD-driven synthetic waveforms to capture the unique transient signatures of gas-entrainment phenomena.
- ix. **Multimodal Data Fusion:** To improve the detection of combined or overlapping fault types, we will integrate additional sensor modalities—such as vibration accelerometers, discharge-pressure transducers, and temperature probes—using data-fusion techniques or a multi-branch deep learning architecture.
- x. **Real-Time, Edge-Optimized Inference:** We plan to explore model-compression techniques (pruning and quantization) and deploy the compressed network on edge platforms (e.g., NVIDIA Jetson, FPGA) to enable low-latency, continuous monitoring without reliance on high-bandwidth data transfers.
- xi. **Cross-Pump Transfer Learning:** To ensure broad applicability across different industrial pumps (submersible, multistage, and positive-displacement), we will apply transfer-learning strategies that adapt our trained model to new pump geometries and operating conditions with minimal additional data.
- xii. **Integration with Maintenance Systems:** Finally, we will embed the diagnostic engine into existing predictive-maintenance workflows, enabling automated alerts, severity-based work orders, and long-term performance analytics for proactive asset management.

By exploring these areas, the effectiveness and applicability of the InceptionV3-based blockage fault diagnosis model for centrifugal pumps can be significantly enhanced, paving the way for more robust and reliable predictive maintenance solutions in the industry.

APPENDIX – A: Deep CNN Basic Structure

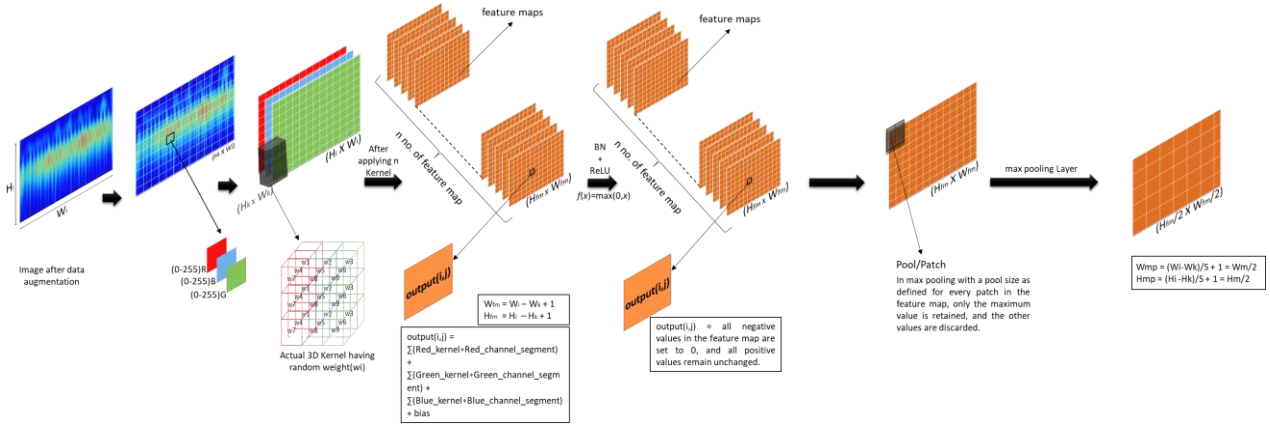


Figure A1: Basics of Convolutional Neural Networks (CNN)

A Convolutional Neural Network (CNN) is a class of deep neural networks commonly used for analyzing visual imagery. The architecture of a CNN is designed to automatically and adaptively learn spatial hierarchies of features from input images. Here is a step-by-step explanation of the CNN process as depicted in the image:

1. Input Image:

The process begins with an input image, which undergoes data augmentation to enhance the diversity of the training set.

2. Convolution Operation:

- The image, represented as a grid of pixel values, is convolved with a set of learnable filters (kernels).
- Each filter slides across the width and height of the image and computes the dot product between the entries of the filter and the input at any position.
- This operation results in a set of feature maps, each corresponding to a filter applied to the input image. Mathematically, this is expressed as:

$$Z_i = \sum (X_i \cdot W_i) + b_i$$

where Z_i is the output feature map, X_i is the input, W_i is the filter, and b_i is the bias term.

3. Activation Function:

- After convolution, an activation function such as ReLU (Rectified Linear Unit) is applied elementwise.
- The ReLU function sets all negative values in the feature maps to zero, while positive values remain unchanged, enhancing non-linearity:

$$f(x) = \max(0, x)$$

4. Pooling (Down sampling):

- Pooling layers are used to reduce the spatial dimensions (height and width) of the feature maps, which decreases the computational cost and helps in making the representation more compact.
- Max pooling is a common technique where the maximum value in each patch of the feature map is selected. If the pool size is $\setminus(S \setminus)$, the pooling operation can be represented as:

$$W_{mp} = \left(\frac{W_i - W_k}{S} + 1 \right) = \frac{W_i}{2}$$

$$H_{mp} = \left(\frac{H_i - H_k}{S} + 1 \right) = \frac{H_i}{2}$$

where W_{mp} and H_{mp} are the pooled width and height.

5. Fully Connected Layers:

- After several convolutional and pooling layers, the high-level reasoning in the neural network is done via fully connected layers. Here, each neuron is connected to every neuron in the previous layer, akin to traditional neural networks.

6. Forward and Backward Propagation:

- In the forward pass, the input data passes through the network layer by layer to produce an output.
- The backward pass involves calculating the gradient of the loss function with respect to each weight by the chain rule, often using techniques like backpropagation. This is essential for updating the weights to minimize the loss function:

$$W_i^* = W_i - \eta \frac{dL}{dW_i}$$

where W_i^* is the updated weight, η is the learning rate, and $\frac{dL}{dW_i}$ is the gradient of the loss with respect to the weight.

This combination of convolutional layers, activation functions, pooling layers, and fully connected layers enables CNNs to effectively learn and capture the intricate patterns and hierarchies in visual data, making them highly effective for tasks such as image classification, object detection, and segmentation.

Derivation of CNN with Batch Normalization, Padding, strides and ReLU Activation Function for Three-Channel Image

Assuming an input image of size 312×312 with 3 channels (RGB), and 35 output classes, let's go through the forward and backward propagation steps, incorporating convolution, batch normalization, padding, and ReLU activation function.

Forward Propagation:

1. Input Image:

$$X \in R^{(312 \times 312 \times 3)}$$

2. Convolutional Layer:

Assume a convolutional layer with F filters, each of size $k_H \times k_W \times 3$, and padding p . The output size is:

$$H_{\text{out}} = \frac{H_{\text{in}} - k_H + 2p}{s} + 1$$

$$W_{\text{out}} = \frac{W_{\text{in}} - k_W + 2p}{s} + 1$$

For simplicity, let's assume stride $s = 1$.

The convolution operation at position (i, j) for the f^{th} filter with padding is:

$$Z_{i,j}^{(f)} = \sum_{m=0}^{k_H-1} \sum_{n=0}^{k_W-1} \sum_{c=0}^2 \widetilde{X_{i+m,j+n,c}} \cdot K_{m,n,c}^{(f)} + b^{(f)}$$

where \widetilde{X} is the padded input image.

3. Batch Normalization:

Batch normalization is applied to the convolution output to normalize the feature maps:

$$\widehat{Z}_{i,j}^{(f)} = \frac{Z_{i,j}^{(f)} - \mu_f}{\sqrt{\sigma_f^2 + \epsilon}}$$

$$\widetilde{Z}_{i,j}^{(f)} = \gamma^{(f)} \widehat{Z}_{i,j}^{(f)} + \beta^{(f)}$$

where μ_f and σ_f^2 are the mean and variance of the feature map, ϵ is a small constant for numerical stability, and $\gamma^{(f)}$ and $\beta^{(f)}$ are learnable parameters.

4. Activation Function (ReLU):

Apply the ReLU activation function elementwise:

$$A_{i,j}^{(f)} = \max(0, \widetilde{Z}_{i,j}^{(f)})$$

5. Pooling Layer:

Assume max pooling with pool size (2×2) and stride 2. The output size is:

$$H_{\text{pooled}} = \left\lfloor \frac{H_{\text{out}}}{2} \right\rfloor$$
$$W_{\text{pooled}} = \left\lfloor \frac{W_{\text{out}}}{2} \right\rfloor$$

The pooling operation is:

$$P_{i,j}^{(f)} = \max(A_{2i,2j}^{(f)}, A_{2i+1,2j}^{(f)}, A_{2i,2j+1}^{(f)}, A_{2i+1,2j+1}^{(f)})$$

6. Fully Connected Layer:

Flatten the pooled output to a vector and pass through fully connected layers. Assume the final layer has 35 neurons (for 35 classes).

Let the flattened vector be f .

The fully connected layer output is:

$$y_i = W_i \cdot f + b_i$$

where W_i is the weight vector for class i .

7. SoftMax Layer:

Apply the SoftMax function to obtain class probabilities:

$$\hat{y}_i = \frac{e^{y_i}}{\sum_{j=1}^{35} e^{y_j}}$$

Backward Propagation:

1. Loss Function:

Use cross-entropy loss function: $L = -\sum_{i=1}^{35} y_i \log(\hat{y}_i)$

2. Gradient of Loss with Respect to Output of SoftMax:

$$\frac{\partial L}{\partial y_i} = \hat{y}_i - y_i$$

3. Gradients in Fully Connected Layer:

$$\frac{\partial L}{\partial W_i} = \frac{\partial L}{\partial y_i} \cdot f$$

$$\frac{\partial L}{\partial b_i} = \frac{\partial L}{\partial y_i}$$

4. Gradients in Pooling Layer:

Since max pooling passes the gradient through the maximum value, backpropagate the gradient to the position of the maximum value in the pooling region.

5. Gradients in Convolutional Layer:

Backpropagate the gradients through the ReLU activation:

$$\frac{\partial L}{\partial \widetilde{Z}_{i,j}^{(f)}} = \frac{\partial L}{\partial A_{i,j}^{(f)}} \cdot \mathbb{1}(\widetilde{Z}_{i,j}^{(f)} > 0)$$

6. Gradients in Batch Normalization:

Backpropagate through batch normalization:

$$\frac{\partial L}{\partial \widetilde{Z}_{i,j}^{(f)}} = \frac{\partial L}{\partial \widetilde{Z}_{i,j}^{(f)}} \cdot \gamma^{(f)} \cdot \frac{1}{\sqrt{\sigma_f^2 + \epsilon}}$$

$$\frac{\partial L}{\partial \gamma^{(f)}} = \sum_{i,j} \frac{\partial L}{\partial \widetilde{Z}_{i,j}^{(f)}} \cdot \widetilde{Z}_{i,j}^{(f)}$$

$$\frac{\partial L}{\partial \beta^{(f)}} = \sum_{i,j} \frac{\partial L}{\partial \widetilde{Z}_{i,j}^{(f)}}$$

7. Gradients in Convolution Weights:

$$\frac{\partial L}{\partial K_{m,n,c}^{(f)}} = \sum_{i,j} \frac{\partial L}{\partial \widetilde{Z}_{i,j}^{(f)}} \cdot \widetilde{X_{i+m,j+n,c}}$$

$$\frac{\partial L}{\partial b^{(f)}} = \sum_{i,j} \frac{\partial L}{\partial \widetilde{Z}_{i,j}^{(f)}}$$

8. Weight Updates:

Update the weights using gradient descent:

$$W_i^* = W_i - \eta \frac{\partial L}{\partial W_i}$$

$$K_{m,n,c}^{(f)} = K_{m,n,c}^{(f)} - \eta \frac{\partial L}{\partial K_{m,n,c}^{(f)}}$$

$$\gamma^{(f)} = \gamma^{(f)} - \eta \frac{\partial L}{\partial \gamma^{(f)}}$$

$$\beta^{(f)} = \beta^{(f)} - \eta \frac{\partial L}{\partial \beta^{(f)}}$$

Here, η is the learning rate.

This detailed derivation covers the entire process of forward and backward propagation for a CNN with convolution, padding, batch normalization, ReLU activation, pooling, and fully connected layers, specifically for an input image of size $312 \times 312 \times 3$ and 35 classes.

References

- [1] Industrial Quick Search, "Editorial by Industrial Quick Search," IQS Directory lists manufacturers and suppliers serving the OEM industrial manufacturing market in the U.S. and Canada. Supported by 208 vertical industry microsites, it aids industrial engineers and buyers in specifying and purchasing products directly. Accessed: Jun. 26, 2024. [Online]. Available: <https://www.iqsdirectory.com/articles/centrifugal-pump.html>
- [2] N. S. Ranawat, A. Miglani, and P. K. Kankar, "Performance of centrifugal pump over a range of composite wear ring clearance," *Journal of the Brazilian Society of Mechanical Sciences and Engineering*, vol. 44, no. 11, Nov. 2022, doi: 10.1007/s40430-022-03835-x.
- [3] P. K. Poonia, "Performance Assessment and Sensitivity Analysis of a Computer Lab Network Through Copula Repair with Catastrophic Failure," *Journal of Reliability and Statistical Studies*, vol. 15, no. 1, pp. 105–127, 2022, doi: 10.13052/jrss0974-8024.1515.
- [4] A. Kumar and R. Kumar, "Time-frequency analysis and support vector machine in automatic detection of defect from vibration signal of centrifugal pump," *Measurement (Lond)*, vol. 108, pp. 119–133, Oct. 2017, doi: 10.1016/j.measurement.2017.04.041.
- [5] N. S. Ranawat, P. K. Kankar, and A. Miglani, "Fault diagnosis in centrifugal pump using support vector machine and artificial neural network," *Journal of Engineering Research (Kuwait)*, vol. 9, pp. 99–111, 2021, doi: 10.36909/jer.EMSME.13881.
- [6] A. K. Panda, J. S. Rapur, and R. Tiwari, "Prediction of flow blockages and impending cavitation in centrifugal pumps using Support Vector Machine (SVM) algorithms based on vibration measurements," *Measurement (Lond)*, vol. 130, pp. 44–56, Dec. 2018, doi: 10.1016/j.measurement.2018.07.092.
- [7] E. J. Grove, R. J. Travis, and S. K. Aggarwal, "Effect of Aging on the PWR Chemical and Volume Control System DISTRIBUTION OF THIS DOCUMENT IS UNLIMITED JU| AQTprj v^V," 1994.
- [8] D. Kumar, A. Dewangan, R. Tiwari, and D. J. Bordoloi, "Identification of inlet pipe blockage level in centrifugal pump over a range of speeds by deep learning algorithm using multi-source data," *Measurement (Lond)*, vol. 186, Dec. 2021, doi: 10.1016/j.measurement.2021.110146.
- [9] R. Tiwari, D. J. Bordoloi, and A. Dewangan, "Blockage and cavitation detection in centrifugal pumps from dynamic pressure signal using deep learning algorithm," *Measurement (Lond)*, vol. 173, Mar. 2021, doi: 10.1016/j.measurement.2020.108676.

- [10] J. S. Rapur and R. Tiwari, "Multifault Diagnosis of Combined Hydraulic and Mechanical Centrifugal Pump Faults Using Continuous Wavelet Transform and Support Vector Machines," *Journal of Dynamic Systems, Measurement and Control, Transactions of the ASME*, vol. 141, no. 11, Nov. 2019, doi: 10.1115/1.4044274.
- [11] N. S. Ranawat, J. Prakash, A. Miglani, and P. K. Kankar, "Performance evaluation of LSTM and Bi-LSTM using non-convolutional features for blockage detection in centrifugal pump," *Eng Appl Artif Intell*, vol. 122, Jun. 2023, doi: 10.1016/j.engappai.2023.106092.
- [12] M. Saberi, A. Azadeh, A. Nourmohammadzadeh, and P. Pazhoheshfar, "Comparing performance and robustness of SVM and ANN for fault diagnosis in a centrifugal pump," in *Chan, F., Marinova, D. and Anderssen, R.S. (eds) MODSIM2011, 19th International Congress on Modelling and Simulation.*, Modelling and Simulation Society of Australia and New Zealand (MSSANZ), Inc., Dec. 2011. doi: 10.36334/modsim.2011.A5.saberi.
- [13] K. C. Luwei, A. Yunusa-Kaltungo, and Y. A. Sha'aban, "Integrated fault detection framework for classifying rotating machine faults using frequency domain data fusion and Artificial Neural Networks," *Machines*, vol. 6, no. 4, 2018, doi: 10.3390/MACHINES6040059.
- [14] S. chikkam and S. Singh, "Condition Monitoring and Fault Diagnosis of Induction Motor using DWT and ANN," *Arab J Sci Eng*, vol. 48, no. 5, pp. 6237–6252, May 2023, doi: 10.1007/s13369-022-07294-3.
- [15] J. Prakash and P. K. Kankar, "Health prediction of hydraulic cooling circuit using deep neural network with ensemble feature ranking technique," *Measurement (Lond)*, vol. 151, Feb. 2020, doi: 10.1016/j.measurement.2019.107225.
- [16] T. N. Babu, P. S. N. Ali, D. R. Prabha, V. N. Mohammed, R. S. Wahab, and S. Vijayalakshmi, "Fault Diagnosis in Bevel Gearbox Using Coiflet Wavelet and Fault Classification Based on ANN Including DNN," *Arab J Sci Eng*, vol. 47, no. 12, pp. 15823–15849, Dec. 2022, doi: 10.1007/s13369-022-06767-9.
- [17] N. S. Ranawat, J. Prakash, A. Miglani, and P. K. Kankar, "Fuzzy Recurrence Plots for Shallow Learning-Based Blockage Detection in a Centrifugal Pump Using Pre-Trained Image Recognition Models," *J Comput Inf Sci Eng*, vol. 23, no. 5, Oct. 2023, doi: 10.1115/1.4062425.
- [18] P. Ma, H. Zhang, W. Fan, C. Wang, G. Wen, and X. Zhang, "A novel bearing fault diagnosis method based on 2D image representation and transfer learning-convolutional neural network," *Meas Sci Technol*, vol. 30, no. 5, Apr. 2019, doi: 10.1088/1361-6501/ab0793.
- [19] M. Mohiuddin, M. S. Islam, S. Islam, M. S. Miah, and M. B. Niu, "Intelligent Fault Diagnosis of Rolling Element Bearings Based on

Modified AlexNet †,” *Sensors*, vol. 23, no. 18, Sep. 2023, doi: 10.3390/s23187764.

- [20] W. Shen, INESC TEC (Organization), Universidade de Trás-os-Montes e Alto Douro, M. IEEE Systems, International Working Group on Computer Supported Cooperative Work in Design, and Institute of Electrical and Electronics Engineers, *Proceedings of the 2019 IEEE 23rd International Conference on Computer Supported Cooperative Work in Design (CSCWD) : May 6-8, 2019, Porto, Portugal*.
- [21] Z. Shang, J. Zhang, W. Li, S. Qian, and M. Gao, “A Domain Adversarial Transfer Model with Inception and Attention Network for Rolling Bearing Fault Diagnosis Under Variable Operating Conditions,” *Journal of Vibration Engineering & Technologies*, vol. 2523, no. 3939, Dec. 2022, doi: 10.1007/s42417-022-00823-2.
- [22] O. Attallah, R. A. Ibrahim, and N. E. Zakzouk, “Fault diagnosis for induction generator-based wind turbine using ensemble deep learning techniques,” *Energy Reports*, vol. 8, pp. 12787–12798, Nov. 2022, doi: 10.1016/j.egy.2022.09.139.
- [23] S. Tang, Y. Zhu, and S. Yuan, “A novel adaptive convolutional neural network for fault diagnosis of hydraulic piston pump with acoustic images,” *Advanced Engineering Informatics*, vol. 52, Apr. 2022, doi: 10.1016/j.aei.2022.101554.
- [24] L. Alzubaidi *et al.*, “Review of deep learning: concepts, CNN architectures, challenges, applications, future directions,” *J Big Data*, vol. 8, no. 1, Dec. 2021, doi: 10.1186/s40537-021-00444-8.
- [25] N. S. Ranawat, A. Miglani, and P. K. Kankar, “Blockage Detection in Centrifugal Pump Using Butterfly Optimization-Based Feature Selection,” *Mapan - Journal of Metrology Society of India*, vol. 38, no. 2, pp. 499–509, Jun. 2023, doi: 10.1007/s12647-022-00616-8.
- [26] M. Pal, P. Manimaran, and P. K. Panigrahi, “A multi scale time–frequency analysis on Electroencephalogram signals,” *Physica A: Statistical Mechanics and its Applications*, vol. 586, Jan. 2022, doi: 10.1016/j.physa.2021.126516.
- [27] A. Akan and O. Karabiber Cura, “Time–frequency signal processing: Today and future,” *Digital Signal Processing: A Review Journal*, vol. 119, Dec. 2021, doi: 10.1016/j.dsp.2021.103216.
- [28] G. Cavazzini, G. Zanetti, A. Santolin, and G. Ardizzone, “Characterization of the hydrodynamic instabilities in a pump-turbine operating at part load in turbine mode,” in *IOP Conference Series: Earth and Environmental Science*, Institute of Physics, 2022. doi: 10.1088/1755-1315/1079/1/012033.
- [29] H. Zhang, R. Yang, and W. He, “Efficacy assessment for multi-vehicle formations based on data augmentation considering reliability,”

- Advanced Engineering Informatics*, vol. 61, Aug. 2024, doi: 10.1016/j.aei.2024.102504.
- [30] M. R. Erick Axel, R. Bustamante-Bello, S. Navarro-Tuch, and H. Perez-Meana, "Applications of the Generalized Morse Wavelets: A Review," 2023, *Institute of Electrical and Electronics Engineers Inc.* doi: 10.1109/ACCESS.2022.3232729.
 - [31] Z. Wei, W. Yang, and R. Xiao, "Pressure Fluctuation and Flow Characteristics in a Two-Stage Double-Suction Centrifugal Pump," *Symmetry (Basel)*, vol. 11, no. 1, p. 65, Jan. 2019, doi: 10.3390/sym11010065.
 - [32] L. P. A. Arts and E. L. van den Broek, "The fast continuous wavelet transformation (fCWT) for real-time, high-quality, noise-resistant time–frequency analysis," *Nat Comput Sci*, vol. 2, no. 1, pp. 47–58, Jan. 2022, doi: 10.1038/s43588-021-00183-z.
 - [33] Z. Nenadic and J. W. Burdick, "Spike detection using the continuous wavelet transform," *IEEE Trans Biomed Eng*, vol. 52, no. 1, pp. 74–87, 2005, doi: 10.1109/TBME.2004.839800.
 - [34] D. Bhatt *et al.*, "Cnn variants for computer vision: History, architecture, application, challenges and future scope," Oct. 01, 2021, *MDPI*. doi: 10.3390/electronics10202470.
 - [35] A. Kerboua and R. Kelaiaia, "Fault Diagnosis in an Asynchronous Motor Using Three-Dimensional Convolutional Neural Network," *Arab J Sci Eng*, 2023, doi: 10.1007/s13369-023-08025-y.
 - [36] S. Naseem, K. Javed, M. J. Khan, S. Rubab, M. A. Khan, and Y. Nam, "Integrated CWT-CNN for epilepsy detection using multiclass EEG dataset," *Computers, Materials and Continua*, vol. 69, no. 1, pp. 471–486, 2021, doi: 10.32604/cmc.2021.018239.
 - [37] C. Szegedy, V. Vanhoucke, S. Ioffe, J. Shlens, and Z. Wojna, "Rethinking the Inception Architecture for Computer Vision," Dec. 2015, [Online]. Available: <http://arxiv.org/abs/1512.00567>
 - [38] C. Nwankpa, W. Ijomah, A. Gachagan, and S. Marshall, "Activation functions: Comparison of trends in practice and research for deep learning," *arXiv preprint arXiv:1811.03378*, 2018.
 - [39] S. F. Stefenon, K. C. Yow, A. Nied, and L. H. Meyer, "Classification of distribution power grid structures using inception v3 deep neural network," *Electrical Engineering*, vol. 104, no. 6, pp. 4557–4569, Dec. 2022, doi: 10.1007/s00202-022-01641-1.
 - [40] L. Li, K. Jamieson, A. Rostamizadeh, and A. Talwalkar, "Hyperband: A Novel Bandit-Based Approach to Hyperparameter Optimization," 2018. [Online]. Available: <http://jmlr.org/papers/v18/16-558.html>.

- [41] X. D. Zhang, "A new method with flexible and balanced control of false negatives and false positives for hit selection in RNA interference high-throughput screening assays," *J Biomol Screen*, vol. 12, no. 5, pp. 645–655, Aug. 2007, doi: 10.1177/1087057107300645.
- [42] D. J. Bordoloi and R. Tiwari, "Identification of suction flow blockages and casing cavitations in centrifugal pumps by optimal support vector machine techniques," *Journal of the Brazilian Society of Mechanical Sciences and Engineering*, vol. 39, no. 8, pp. 2957–2968, Aug. 2017, doi: 10.1007/s40430-017-0714-z.
- [43] J. S. Rapur and R. Tiwari, "Automation of multi-fault diagnosing of centrifugal pumps using multi-class support vector machine with vibration and motor current signals in frequency domain," *Journal of the Brazilian Society of Mechanical Sciences and Engineering*, vol. 40, no. 6, Jun. 2018, doi: 10.1007/s40430-018-1202-9.